



Linear Spectral Mixing Model: Theoretical Concepts, Algorithms and Applications of Studies in the Legal Amazon

Modelo Linear de Mistura Espectral: Conceitos Teóricos, Algoritmos e Aplicações em Estudos na Amazônia Legal

Yosio Edemir Shimabukuro 1, Andeise Cerqueira Dutra 2 e Egidio Arai 3

1 Instituto Nacional de Pesquisas Espaciais (INPE), Divisão de Observação da Terra e Geoinformática (DIOTG), São José dos Campos, SP, Brasil, E-mail. yosio.shimabukuro@inpe.br

ORCID: <https://orcid.org/0000-0002-1469-8433>

2 Instituto Nacional de Pesquisas Espaciais (INPE), Divisão de Observação da Terra e Geoinformática (DIOTG), São José dos Campos, SP, Brasil, E-mail. andeise.dutra@inpe.br

ORCID: <https://orcid.org/0000-0002-4454-7732>

3 Instituto Nacional de Pesquisas Espaciais (INPE), Divisão de Observação da Terra e Geoinformática (DIOTG), São José dos Campos, SP, Brasil, E-mail. egidio.arai@inpe.br

ORCID: <https://orcid.org/0000-0003-1994-5277>

Received: 08.2020 | Accepted: 11.2020

Abstract: This paper presents a review of the Linear Spectral Mixing Model and its applications in the Legal Amazon. Studies on spectral mixture began in the 1970s, motivated by the problem of area estimation obtained by automatic interpretation. The pixel was classified or not based on the maximum probability of this pixel to belong to a given class, then overestimating or underestimating this class according to the decision made. Thus, interest in the study of the spectral mixture within the pixel arose. The response of each pixel can be considered as a linear combination of the spectral responses of each component that is within the pixel. Thus, knowing the spectral responses of the components, we can obtain the proportions of these components (fraction images). This paper presents the theoretical concepts that motivated the development of this model, and the algorithms (Constrained Least Squares, Weighted Least Squares, Principal Components) developed in the 1980s are described. With the availability of these algorithms in the digital image processing software in the 1990s, the number of studies using this technique increased in Brazil and worldwide. The fraction images were used to automate the PRODES Project (Monitoring deforestation of the Brazilian Amazon Forest by Satellite) which was the first systematic operational project of orbital Remote Sensing. Following the use of fraction images in studies conducted in the Brazilian Amazon are presented. In addition, a perspective of use of fraction images for global studies is presented. In conclusion, the Linear Spectral Mixture Model has contributed to the development of several research and applications of Remote Sensing due to its data reduction characteristics and by highlighting the targets of interest in the images.

Keywords: Constrained Least Squares. Deforestation. Selective Logging. Burning. Land Use and Land Cover.

Resumo: Este trabalho apresenta uma revisão sobre o Modelo Linear de Mistura Espectral e suas aplicações na Amazônia Legal. Os estudos sobre mistura espectral iniciaram na década de 1970, motivada pelo problema na estimativa de áreas obtida por interpretação automática. O pixel era classificado ou não baseado na máxima probabilidade desse pixel pertencer a determinada classe, superestimando ou subestimando esta classe de acordo com a decisão tomada. Surgiu então o interesse no estudo da mistura espectral dentro do pixel. A resposta de cada pixel pode ser considerada como uma combinação linear das respostas espectrais de cada componente que está na mistura desse pixel. Dessa forma, conhecendo-se as respostas espectrais dos componentes, podemos obter as proporções desses componentes (imagens fração). Neste trabalho são apresentados os conceitos teóricos que motivaram o desenvolvimento desse modelo, e são descritos os algoritmos (Mínimos Quadrados com Restrição, Mínimos Quadrados Ponderados, Principais Componentes) desenvolvidos na década de 1980. Com a disponibilidade desses algoritmos em softwares de processamento de imagens digitais na década de 1990, aumentou o número de trabalhos que fazem uso dessa técnica no Brasil e no mundo. As imagens fração foram utilizadas para automatizar o Projeto PRODES (Monitoramento do Desmatamento da Floresta Amazônica Brasileira por Satélite) que foi o primeiro projeto operacional sistemático de Sensoriamento Remoto orbital. A seguir é apresentada a utilização das imagens fração em estudos realizados na Amazônia brasileira. Além disso, é apresentada uma perspectiva de uso das imagens fração em estudos globais. Em conclusão, o Modelo Linear de Mistura Espectral tem contribuído para o desenvolvimento de várias pesquisas e aplicações de Sensoriamento Remoto devido as suas características de redução de dados e por realçar os alvos de interesse nas imagens.

Palavras-chave: Mínimos Quadrados com Restrição. Desmatamento. Corte Seletivo. Queimada. Uso e Cobertura da Terra.

1 INTRODUCTION

The phenomenon of "spectral mixture" has been considered by some researchers in the field of remote sensing (HORWITZ et al., 1971; DETCHMENDY; PACE, 1972; HEIMES, 1977; SHIMABUKURO, 1987). Usually, the problem arises when trying to correctly classify a pixel that contains a mixture of materials on the surface such as soil, vegetation, rocks, water, and others. The non-uniformity of most natural scenarios usually results in a large number of components in the mixture. The spectral mixture problem becomes more critical for digital processing techniques than for visual interpretation by trained interpreters. Interpreters basically use three fundamental standard elements – spectral, spatial, and contextual characteristics (PANIZZA; FONSECA, 2011) – to extract information from aerial and satellite images, while most digital analysis techniques are predominantly based on the spectral characteristics of the pixels.

The spectral mixture process can occur regardless of the spatial resolution of the sensor, so the pixel mixture problem is not solved simply by increasing the spatial resolution (KESHAVA; MUSTARD, 2002). For example, in high spatial resolution images of a forest canopy, elements such as shadow and gaps become apparent, collaborating for the mixture inside the image pixel.

Several mathematical formulations to solve the spectral mixture of materials within pixels have been reported in the literature. Horwitz et al. (1971) used a nonlinear programming algorithm to extract the components of the mixture. The least-square procedure with constraints was proposed by Detchmendy and Pace (1972), while Hallum (1972) expanded Detchmendy and Pace's (1972) set of solutions by incorporating the proportions constraints.

However, the spectral mixture model was not actually employed in remote sensing until the mid-1980s (SMITH et al., 1985; ADAMS et al., 1986; SHIMABUKURO, 1987). Since then, interest in the spectral mixture (linear and nonlinear) has increased considerably and several studies have been developed using this technique (BOARDMAN; 1993; ROBERTS et al., 1993; FARRAND et al., 1994; ATKINSON et al., 1997; BASTIN, 1997; FOODY et al., 1997; NOVO; SHIMABUKURO, 1994; SHIMABUKURO; SMITH, 1995; ROSIN, 2001; GARCÍA-HARO et al., 2005; ALCÂNTARA et al., 2009). The developed models have been applied to images obtained by the various Earth observation satellites. These models estimate the proportions of components within pixels generating fraction images corresponding to the components of those pixels. In general, the pixel mixture is commonly formed by the components of high albedo and low albedo, and can then represent, respectively, soil, vegetation, and shade fraction images. These fraction images have been used in various research areas such as forest resources, agricultural, urban, and flooded areas, etc. In addition, these fraction images were important for the creation of operational projects for estimating deforested areas (PRODES) (SHIMABUKURO et al., 1998), detection of deforested areas in near-real-time (DETER) (ANDERSON et al., 2005; SHIMABUKURO et al., 2006), and have been used in numerous research works in the Amazon region.

In this context, the objective of this work is to present a review of the Linear Spectral Mixing Model. Thus, the theoretical concepts, mathematical algorithms, and examples of applications in the Amazon region are presented.

2 THEORETICAL CONCEPTS

The brightness recorded in the satellite images is an integrated sum of the brightness of all targets within the instantaneous field of view (IFOV) of the remote sensors. Thus, the radiation detected is caused by a mixture of several different materials within the image pixels (SHIMABUKURO, 1987; SHIMABUKURO; SMITH, 1991). In this way, numerous different materials often contribute to the spectrum recorded in an image pixel acquired by satellite sensors. Thus, the identification of the individual constituent materials presented in the mixture and the proportions in which they appear is important to analyze the images, since

the mixture may result in overestimation or underestimation of the area in automatic classifications, according to the higher or lower probability of this pixel to belong to one of these materials (SHIMABUKURO, 1987).

The mixture of different materials or objects contained "within" the pixel at the time of measuring the intensity of radiant flux by a sensor, happens when different objects are instantly viewed in a portion of the land surface with well-defined dimensions. It is known that the radiation flux originated by the incident radiation reflection is actually a mixture of different radiation fluxes that results in a single measure of intensity by the sensors in each spectral region of the electromagnetic spectrum.

The concept of spectral mixture was discussed by Horwitz et al. (1971), Detchmندی and Pace (1972), Ranson (1975), and Heimes (1977), among others. The Spectral mixture can occur in two cases: 1) when materials (or objects) are smaller than the pixel size, i.e., the radiation flux detected by the sensor is composed of a mixture of radiation from all materials within the pixel; and 2) when the pixel overlaps the edge between two or more materials or objects larger than the pixel size (SHIMABUKURO, 1987). In both cases, the signals recorded by the sensor are not representative of anyone of the materials present inside the pixel. Thus, the spectral mixing is the procedure when the measured spectrum of a mixture pixel is decomposed into a collection of constituent spectra, or endmembers, and a set of corresponding proportions or abundances that indicate the contribution of each endmember present in the pixel (KESHAVA, 2003).

The mixing process can be considered linear or nonlinear. The combination will be basically linear if the endmembers in a pixel appear in spatially segregated patterns. In this case, the dispersion and absorption of incident radiation in any region on the surface are dominated by a single component on the land surface. Thus, the spectrum of a mixed pixel can be considered a linear combination of the spectrum weighted by the fractional area coverage of each endmember within the pixel (HAPKE, 1993). However, if the components of interest are in a circumstantial association, electromagnetic radiation will typically interact with more than one component (such as sand grains of different compositions on a beach) and the mixing process between these different components will be nonlinear as a result of the interaction of multiple dispersion. An example of nonlinear mixing is the interleaving of different types of vegetation in the tree canopies (ROBERTS et al., 1993).

The linear approach has been demonstrated in numerous applications because it is considered a useful technique for interpreting variability in remote sensing data and a powerful way to convert spectral information into data products with physical meaning, such as the abundance of materials on the land surface (KESHAVA; MUSTARD, 2002).

Given the importance of the linear spectral mixing model and the range of applications, several review works have been presented in the literature describing the existing algorithms to generate fraction images (ADAMS et al., 1995; ICHOKU; KARNIELI; 1996; KESHAVA; MUSTARD, 2002; PLAZA et al., 2002; KESHAVA, 2003; PLAZA et al., 2004; ADAMS; GILLESPIE, 2006; QUINTANO et al., 2012).

Generally, the linear spectral mixing model can be written as Eq. (1):

$$r_i = \sum_{j=1}^m x_j a_{i,j} + e_i \quad (1)$$

where:

r_i = spectral reflectance of the pixel for the i th spectral band;

a_{ij} = spectral reflectance of the j th component in the pixel for the i th spectral band;

x_j = proportion value of the j th component in the pixel;

e_i = error for the i th spectral band;

$j = 1, 2, \dots, m$ (m = number of components considered in the pixel);

$i = 1, 2, \dots, n$ (n = number of spectral bands of the sensor).

As mentioned earlier, this model assumes that the spectral response (in Eq. (1), expressed as reflectance) of pixels are linear combinations of spectral responses of components within the pixel. To solve

Eq. (1), it is necessary to have the spectral reflectance of the pixels (r_i) in each band and the spectral reflectance of each component (a_{ij}) in each band to estimate the proportion values, or vice versa.

For the solution of the system of linear equations that represents the spectral mixing model in question, there are several mathematical approaches based on the least squares method. Following it will be presented three algorithms available in the image processing software (SPRING, ENVI and PCI) (SHIMABUKURO; PONZONI, 2017).

3 MATHEMATICAL ALGORITHMS

The percentages of each object within a pixel can take multiple dimensions, depending on the spatial resolution of each sensor. These proportions are calculated by applying mathematical models. In this work, linear models will be presented, but it is important to be aware that linearity may not be the only way to describe the participation of each object in a pixel. The Linear spectral mixing model (LSMM) will be described since it is widely used by researchers with consistent results.

Following this approach, the spectral response in each pixel, in any sensor spectral band, can be imagined as a linear combination of the spectral responses of each component present in the mixture. Thus, each pixel, which can assume any value within the gray level range of the image, contains information about the proportion (quantity) and the spectral response of each component within a spatial resolution element (pixel) on the ground. Therefore, for any multispectral image generated by any sensor system, considering the knowledge of the proportion of components, it will be possible to estimate the spectral response of each of these components. Similarly, if this response is known, the proportion of each component in the mixture can be estimated. This feature helps in the analysis of different sensors with different spatial resolutions. For example, it is possible to generate fraction images from a sensor with high spatial resolution and, based on these proportions, to estimate the spectral responses of the objects present in the pixels generated by a medium spatial resolution sensor, and then generate the fraction images for the moderate and low spatial resolution sensor images (SHIMABUKURO; SMITH, 1995; DUTRA et al., 2019).

The linear spectral mixing model is a system of equations, with an equation for each band of the sensor. For example, for MSS (Multi Spectral Scanner) sensor, onboard Landsat 1-5 satellites, there are four equations, corresponding to bands 4, 5, 6 and 7, while for TM (Thematic Mapper) sensor onboard Landsat 4 and 5 satellites there are six equations, corresponding to bands 1, 2, 3, 4, 5 and 7, taking into account only the solar optical spectrum. It is important to keep in mind that it is not necessary to use all available bands, but it must obey the condition that the number of reference spectra (or pure pixels) is always less than the number of spectral bands. Thus, mathematical algorithms are necessary for the solution of the system of equations formed by the spectral response of the pixel, which is the function of the proportion of each reference spectrum (or pure pixels) weighted by the respective spectral response of the component. Following it will be presented three mathematical algorithms: Constrained Least Squares (CLS), Weighted Least Squares (WLS), and Principal Components (PC) (SHIMABUKURO; PONZONI, 2017).

3.1 Constrained Least Squares

The CLS method estimates the proportion of each component within the pixel, minimizing the sum of squared errors. The proportion values obtained by this algorithm should result in non-negative numbers (physical meaning) and the sum equal to 1. To solve this problem, a nearly closed solution method was developed (for example, a method that finds the solution by making approximations that satisfy these constraints). As example, the proposed method will be presented for the case of three components ($m=3$) within the pixel. It is important to remember that this model can be developed for a larger number of endmembers, but that the solution will become increasingly complex. Thus, the mixture model, wrote in the Eq. (1) can be re-written as Eq. (2):

$$e_i = r_i - \sum_{j=1}^m x_j a_{i,j} \tag{2}$$

In this case we will use $n = 4$ spectral bands and $m = 3$ components within the pixel. The function to be minimized can be written as Eq. (3) or Eq. (4):

$$F = \sum e_i^2 \tag{3}$$

or

$$e_1^2 + e_2^2 + e_3^2 + e_4^2 = E_1 x_1^2 + E_2 x_2^2 + E_3 x_3^2 + E_4 x_1 x_2 + E_5 x_1 x_3 + E_6 x_2 x_3 + E_7 x_1 + E_8 x_2 + E_9 x_3 + E_{10} \tag{4}$$

The values of coefficients E_1 to E_{10} are shown in Chart 1.

Chart 1 - Values of coefficients E_1 to E_{10} for Eq. (4).

$E_1 = a_{11}^2 + a_{21}^2 + a_{31}^2 + a_{41}^2$ $E_2 = a_{12}^2 + a_{22}^2 + a_{32}^2 + a_{42}^2$ $E_3 = a_{13}^2 + a_{23}^2 + a_{33}^2 + a_{43}^2$ $E_4 = 2x (a_{11} a_{12} + a_{21} a_{22} + a_{31} a_{32} + a_{41} a_{42})$ $E_5 = 2x (a_{11} a_{13} + a_{21} a_{23} + a_{31} a_{33} + a_{41} a_{43})$ $E_6 = 2x (a_{12} a_{13} + a_{22} a_{23} + a_{32} a_{33} + a_{42} a_{43})$ $E_7 = -2x (a_{11} r_1 + a_{21} r_2 + a_{31} r_3 + a_{41} r_4)$ $E_8 = -2x (a_{12} r_1 + a_{22} r_2 + a_{32} r_3 + a_{42} r_4)$ $E_9 = -2x (a_{13} r_1 + a_{23} r_2 + a_{33} r_3 + a_{43} r_4)$ $E_{10} = r_1^2 + r_2^2 + r_3^2 + r_4^2$
--

Source: Shimabukuro and Ponzoni (2017).

Consider the first constraint: $x_1 + x_2 + x_3 = 1$ or $x_3 = 1 - x_1 - x_2$. Replacing this restriction in the Eq. (4), the function to be minimized becomes as Eq. (5):

$$e_1^2 + e_2^2 + e_3^2 + e_4^2 = A_1 x_1^2 + A_2 x_2^2 + A_3 x_1 x_2 + A_4 x_1 + A_5 x_2 + A_6 \tag{5}$$

The values of coefficients A_1 to A_6 are shown in Chart 2.

Chart 2 - Values of Coefficients A_1 to A_6 for Eq. (5).

$A_1 = a_{11}^2 + a_{21}^2 + a_{31}^2 + a_{41}^2 + a_{13}^2 + a_{23}^2 + a_{33}^2 + a_{43}^2 - 2x (a_{11} a_{13} + a_{21} a_{23} + a_{31} a_{33} + a_{41} a_{43})$ $A_2 = a_{12}^2 + a_{22}^2 + a_{32}^2 + a_{42}^2 + a_{13}^2 + a_{23}^2 + a_{33}^2 + a_{43}^2 - 2x (a_{12} a_{13} + a_{22} a_{23} + a_{32} a_{33} + a_{42} a_{43})$ $A_3 = 2 (r_1^2 r_2^2 + a_{23}^2 + a_{33}^2 + a_{43}^2 + a_{11} a_{12} + a_{21} a_{22} + a_{31} a_{32} + a_{41} a_{42} - a_{11} a_{13} - a_{21} a_{23} - a_{31} a_{32} - a_{41} a_{43} - a_{12} a_{13} - a_{22} a_{23} - a_{32} a_{33} - a_{42} a_{43})$ $A_4 = 2 (- a_{13}^2 - a_{23}^2 - a_{33}^2 - a_{43}^2 + a_{11} a_{13} + a_{21} a_{23} + a_{31} a_{33} + a_{41} a_{43} - a_{11} r_1 - a_{21} r_2 - a_{31} r_3 - a_{41} r_4 + a_{13} r_1 + a_{23} r_2 + a_{33} r_3 + a_{43} r_4)$ $A_5 = 2 (- a_{13}^2 - a_{23}^2 - a_{33}^2 - a_{43}^2 + a_{12} a_{13} + a_{22} a_{23} + a_{32} a_{33} + a_{42} a_{43} - a_{12} r_1 - a_{22} r_2 - a_{32} r_3 - a_{42} r_4 + a_{13} r_1 + a_{23} r_2 + a_{33} r_3 + a_{43} r_4)$ $A_6 = a_{13}^2 + a_{23}^2 + a_{33}^2 + a_{43}^2 + r_1^2 + r_2^2 + r_3^2 + r_4^2 - 2 x (a_{13} r_1 + a_{23} r_2 + a_{33} r_3 + a_{43} r_4)$

Source: Shimabukuro and Ponzoni (2017).

In this manner, the function to be minimized is rewritten as Eq. (6):

$$F = A_1 x_1^2 + A_2 x_2^2 + A_3 x_1 x_2 + A_4 x_1 + A_5 x_2 + A_6 \tag{6}$$

where coefficients A_1 to A_6 are functions of spectral values, a_{ij} (endmembers response values) and r_i (pixel response values).

To solve this problem, it is necessary to find a minimum value within the area defined by the lines: $0 \leq x_1 \leq a$, $0 \leq x_2 \leq b$, and $\frac{x_1}{a} + \frac{x_2}{b} = 1$, in which $a = b = 1$ (Figure 1). Considering the function to be minimized, in order to find the minimum value, the partial derivatives are calculated and equaled to zero, as written in Eq. (7) and in Eq. (8):

$$\frac{dF}{dx_1} = 2A_1 x_1 + A_2 x_2 + A_4 = 0 \tag{7}$$

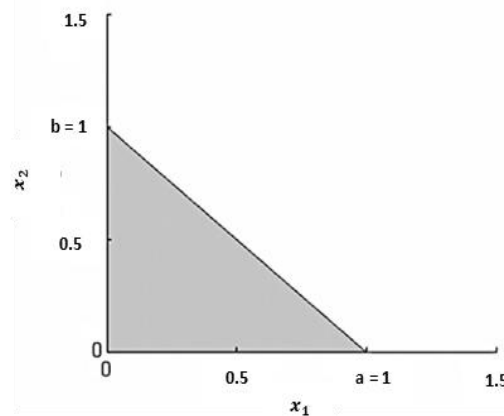
$$\frac{dF}{dx_2} = 2A_2 x_2 + A_3 x_1 + A_5 = 0 \tag{8}$$

Solving for x_1 and x_2 , written as Eq. (9) and Eq. (10), respectively:

$$x_1 = \frac{(A_3 A_5 - 2A_2 A_4)}{(4A_1 A_2 - A_3^2)} \tag{9}$$

$$x_2 = \frac{(A_3 A_4 - 2A_1 A_5)}{(4A_1 A_2 - A_3^2)} \tag{10}$$

Figure 1 - Region that meets the constraints for the number of components equal to three.



Source: Shimabukuro and Ponzoni (2017).

So, there are five possible situations, which are described below:

- Situation 1, where the minimum value is within the region of interest. This is the final solution and $x_3 = 1 - x_1 - x_2$;
- Situation 2, where the minimum value is outside the region and x_1 and x_2 are positive. In this case, the minimum restricted value is searched on the line defined by $x_1 + x_2 = 1$ (i.e., $x_3 = 0$). Now, by making $x_2 = 1 - x_1$, the function to be minimized can be written as Eq. (11):

$$F = (A_1 + A_2 - A_3) x_1^2 + (A_3 + A_4 - A_5 - 2A_2) x_1 + (A_2 + A_5 + A_6) \tag{11}$$

The minimum value will be obtained, as written in Eq. (12) and in Eq. (13):

$$\frac{dF}{dx_1} = 2(A_1 + A_2 - A_3) x_1 + (A_3 + A_4 - A_5 - 2A_2) = 0 \tag{12}$$

So:

$$x_1 = \frac{-(A_3 + A_4 - A_5 - 2A_2)}{(2(A_1 + A_2 - A_3))} \tag{13}$$

If $x_1 > 1$, make $x_1 = 1$, or, if $x_1 < 0$, make $x_1 = 0$ and $x_2 = 1 - x_1$;

- Situation 3, where the minimum value is outside the region and x_1 is negative and x_2 is positive. In this case, by making $x_1 = 0$, the function to be minimized becomes as Eq. (14):

$$F = A_2 x_2^2 + A_5 x_2 + A_6 \tag{14}$$

Solving to find the minimum, $x_2 = \frac{-A_5}{2A_2}$. If $x_2 > 1$, then make $x_2 = 1$, or, if $x_2 < 0$, make $x_2 = 0$ and $x_3 = 1 - x_2$;

- Situation 4, where the minimum value is outside the region and x_1 and x_2 are negative. In this case, x_1 and x_2 are equal to zero and $x_3 = 1$;
- Situation 5, where the minimum value is outside the region and x_1 is positive and x_2 is negative. In this case, by making $x_2 = 0$, the function to be minimized becomes as Eq. (15):

$$F = A_1 x_1^2 + A_4 x_1 + A_6 \tag{15}$$

Solving to find the minimum, $x_1 = \frac{-A_4}{2A_1}$. If $x_1 > 1$, then $x_1 = 1$, or if $x_1 < 0$, then $x_1 = 0$ and $x_3 = 1 - x_1$.

3.2 Weighted Least Squares

Consider the curve that fits the data in the format as Eq. (16):

$$R = f(A, x_1, x_2, \dots, x_m) = x_1 f(A) + x_2 f(A) + \dots + x_m f(A) \tag{16}$$

where the dependent variable R is linear in relation to x_1, x_2, \dots, x_m .

Although there are many branches and approaches to curve adjustment, the least squares method can be applied to a wide variety of curve adjustment problems involving the linear shape with indeterminate values. Values are determined by minimizing the sum of squared errors (residuals). The solution obtained by this method is mathematically possible, but it can be physically unacceptable (some constraints are involved: the values should not be negative, and the sum must be equal to 1). Then, it becomes a problem of constrained least squares, and constraint equations must be added. To solve this problem, it is necessary to apply the weighted least squares concepts.

Sometimes the information obtained in an experiment can be more accurate than that resulting from other sources of information related to the same experiment. In other cases, we should use some additional information (previous knowledge) to make the solution physically relevant. In such cases, it may be desirable to assign a greater "weight" to the information considered more accurate or more important to the problem. Giving certain weights (e.g. additional information) is desirable to bring the solution closer to the physical meaning and obtain an acceptable solution.

In this case, $x_1 + x_2 + \dots + x_m = 1$ and $0 \leq x_1, x_2, \dots, x_m \leq 1$ are the conditions that must be met to get an acceptable solution. So, $r + 1$ equations are added to the system of Eq. 10: one corresponding to the conditional sum of proportions equal to 1 ($x_1 + x_2 + \dots + x_m = 1$) and r equations corresponding to the

condition that the proportions are not negative ($0 \leq x_j \leq 1, j = 1, 2, \dots, m$). To solve this problem, when constraints are not met, a W diagonal matrix containing weight values associated with the system of equations to be solved is applied. Initially, the first assigned values are equal to 1 along the diagonal W matrix, meaning that the equations are equally important for solving the problem. Very high value assigned to the diagonal corresponding to the first constraint (sum of $x_j = 1$) indicates that this equation must be strictly satisfied. Therefore, if the x_j values are satisfied, that is, if they are in the range between 0 and 1, the final solution was achieved. Otherwise, it is necessary to use an iterative process to place all x_j within the range between 0 and 1. This is achieved by a gradual increase in weights, which are initially zero, corresponding to the most recent equations related to the restriction that the proportions should not be negative. The solution to this problem is found by minimizing the amount: $w_1 e_1^2 + w_2 e_2^2 + \dots + w(n + m + 1)$ and $(n + m + 1)^2$, where w_1, w_2 , etc. are the weight factors and e_1, e_2 , etc. are the error values for each equation.

The implementation of this method is based on the Gaussian elimination and substitution algorithm, described in the numerical analysis textbooks such as Burden, Faires and Reynolds (1981).

3.3 Principal Components

Given an image consisting of a number of pixels measured in multiple spectral bands, it is possible to model each spectral response of each pixel as a linear combination of a finite number of components, as written in Eq. (17).

$$\begin{aligned}
 dn_1 &= f_1 e_{1,1} + \dots + f_n e_{1,m} && \text{band 1} \\
 dn_2 &= f_1 e_{2,1} + \dots + f_n e_{2,m} && \text{band 2} \\
 &\dots && \\
 dn_p &= f_1 e_{p,1} + \dots + f_n e_{p,m} && \text{band } p
 \end{aligned}
 \tag{17}$$

where:

dn_i = spectral response of the pixel in band i ;

e_{ij} = spectral response of the pure component j in band i ;

f_j = unknown fraction of the pure component j ;

m = number of pure components;

p = number of bands.

In this way, the equation can be in a matrix form written as Eq. (18):

$$dn = e f
 \tag{18}$$

A linear constraint is added because the sum of fractions of any pixel must be equal to 1; therefore, it is necessary to increase the dn vector with a line of values of 1. This becomes a set of equations $p + 1$ in m unknowns. Because the number of pure components is generally less than the number of spectral bands, equations can be solved by any technique. The described solution uses Principal Component Analysis (PCA) to reduce the dimensionality of the dataset. The pure component matrix is transformed into a PCA space using the appropriate number of autovectors, pixel data is transformed into PCA space, solutions are achieved, and the resulting fractions are stored (SMITH et al., 1985).

The Weighted Least Squares and the Principal Component methods are recommended when the number of spectral components in the mixture is greater than three (SHIMABUKURO; PONZONI, 2017).

4 ENDMEMBERS SELECTION

To generate fraction images, it is necessary to choose pure components (endmembers) to apply any

available mathematical algorithm. Explicitly defined, the endmember is just a component that is part of the spectral mixture, i.e., it is part of the pixel. Thus, it is necessary to choose the endmembers that make sense for interpretation of the image and that also meet the criteria of the fraction according to the equations of the spectral mixture. Sometimes it is easy to choose these endmembers when the spectral behavior of targets is already known for the area being studied. This occurs in areas that have been studied for some time, such as when changes in the environment are being monitored. On the other hand, it is necessary to perform experiments to find the appropriate endmembers whenever the scenes are unknown or when it is necessary to extract specific information from the images.

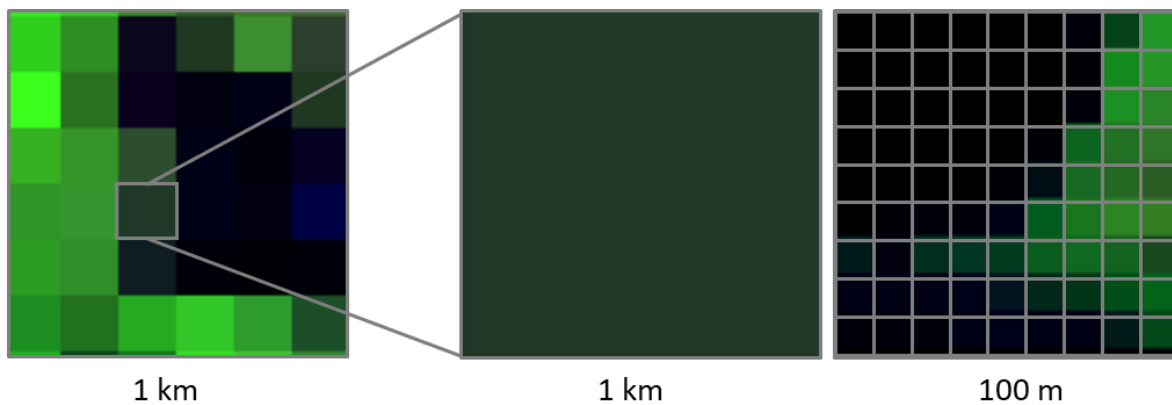
There are two ways to select endmembers: extracting spectral values directly from images or by collecting data obtained in laboratory and/or in the field using spectroradiometers. Endmembers derived from images are called image endmembers, while those selected from laboratory and/or in the field are called reference endmembers. The most convenient is to select the endmembers directly from the images being studied for the simple reason that the spectrum of the endmember extracted from the image can be used without image calibration. On the other hand, the spectra obtained in laboratory or in the field present values of reflectance factors. As known, orbital images are in principle available in DN (Digital Number) format. Thus, the reference endmembers (reflectance factors) would be at scale or in a unit different from that adopted by the images (DNs), which would interfere in the application of the mixing model. The correct procedure would be to convert the DNs of the images into surface reflectance factors, with atmospheric correction, in order to have compatibility in the unit of the two datasets, that is already currently occurring with the availability of vast majority of free orbital products (e.g.: Landsat series and MODIS).

Although image endmember is convenient by not requiring calibration it does not always work on mixing models. To work well, it is necessary to have a good agreement between the pixel scale and the scale in which materials occur relatively pure on the ground. At best hypothesis, the image endmember can be used if the study image has at least a few pixels fully occupied by a single material on the land surface.

It can be concluded in a more or less intuitive way that the definition of the number and selection of endmembers are essential for the success of the mixing model. However, it is known that, in a real world, the terrain can be spectrally complex. One reason why an image can be well modeled by few endmembers spectra is due to the fact that some potential endmembers are in small proportions on the land surface compared to the major endmembers considered in the mixture pixel.

When considering the use of image endmembers, it is assumed that in high- and medium- spatial resolution images there is a high probability of finding pure pixels or pixels that include a single component available in the image. However, in the moderate and low spatial resolution images, the mixed nature of pixels limits this approach due to the difficulty or even the impossibility of obtaining pure pixels (SHIMABUKURO; SMITH, 1995; DE FREITAS et al., 2008). Particularly in a global or regional scale studies, the determination of these endmembers remains a challenge (MEYER; OKIN, 2015). From this perspective, some studies propose to estimate the spectral responses of endmembers in images of low spatial resolution, from the proportions obtained from the images of higher spatial resolution (Figure 2) using regression models (SHIMABUKURO; SMITH, 1995; DE FREITAS et al., 2008; DUTRA et al., 2019). Assuming that the spectral response of a pixel can be obtained as a linear combination of the responses of each element contained within it, each pixel contains information about the proportion and spectral response of each component (SHIMABUKURO; SMITH, 1991).

Figure 2 - Representation of a pixel with spatial resolution of 1km and the same coverage area in 100 m pixels obtained from the same PROBA-V satellite.



Source: Dutra et al. (2019).

5 FRACTION IMAGES

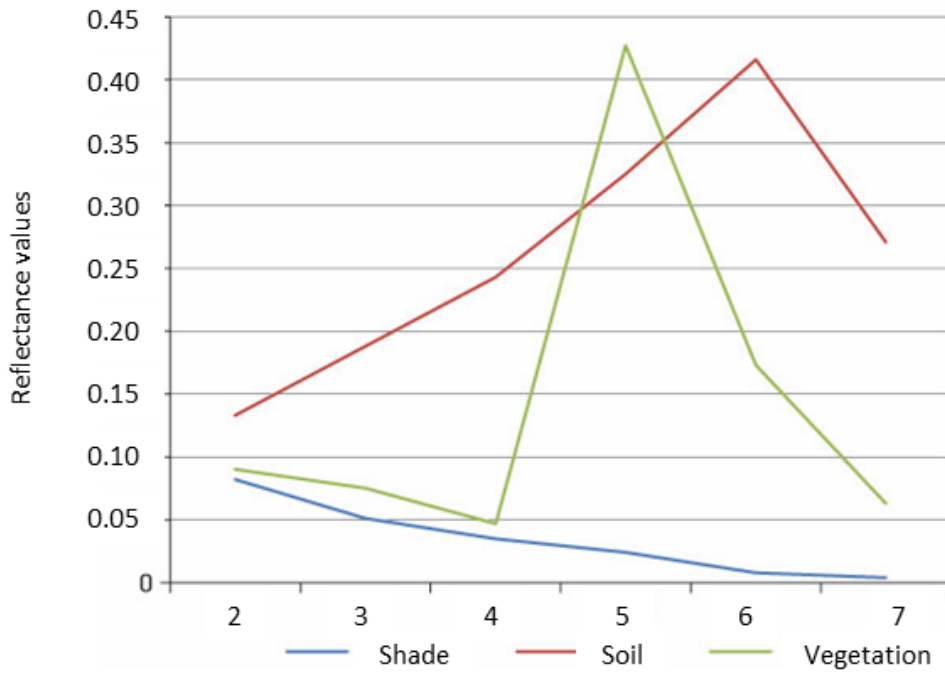
Fraction images are the products generated from application of the mathematical algorithms described earlier. They are represented by images in which the pixel value corresponds to the proportions of the components considered in the spectral mixture. In general, all algorithms produce the same result, that is, they generate the same fraction images when constraint equations are not used, i.e., the proportions are in the range of 0 to 1. Typically, fraction images of vegetation, soil, and shade/water are generated, which are the components usually present in any scene on the land surface. Fraction images can be considered as a way of reducing the dimensionality of the data and also a way of highlighting the information. In addition, the spectral mixing model transforms spectral information into physical information (component proportion values in the pixel).

The vegetation fraction image highlights the vegetation cover areas, the soil fraction image highlights the exposed soil areas, and the shade/water fraction image highlights the areas occupied by water bodies, such as rivers and lakes, as well as burned areas, wetlands, etc. Shade and water are considered together because these two targets exhibit similar responses in spectral bands normally used by Earth observation sensors, such as low spectral response in the spectral regions. Thus, it is important to note that the spectral mixing model is not a classifier, but an image transformation technique to facilitate information extraction (SHIMABUKURO; PONZONI, 2017).

Figure 3 shows an example of the spectral responses of the components of vegetation, soil, and shade/water used to generate fraction images in a scene with path 231 and row 062 of an image from the OLI (Operational Land Imager) sensor onboard Landsat-8 satellite, corresponding to Manaus region (Amazon State). In this case, the images of all bands were used as example: 1 ($0.43 \mu\text{m} - 0.45 \mu\text{m}$), 2 ($0.45 \mu\text{m} - 0.51 \mu\text{m}$), 3 ($0.52 \mu\text{m} - 0.60 \mu\text{m}$), 4 ($0.63 \mu\text{m} - 0.68 \mu\text{m}$), 5 ($0.84 \mu\text{m} - 0.88 \mu\text{m}$), 6 ($1.56 \mu\text{m} - 1.66 \mu\text{m}$) and 7 ($2.10 \mu\text{m} - 2.30 \mu\text{m}$), which were previously converted into surface reflectance values. It is worth remembering that this analysis can be performed using the apparent or surface reflectance values or even DNs as long as the spectrum of the components is obtained from these images. Figure 4A shows a color composite (R6 G5 B4) of OLI/Landsat-8 sensor images, while figures 5B to 5G show the images corresponding to the spectral bands 2 to 7.

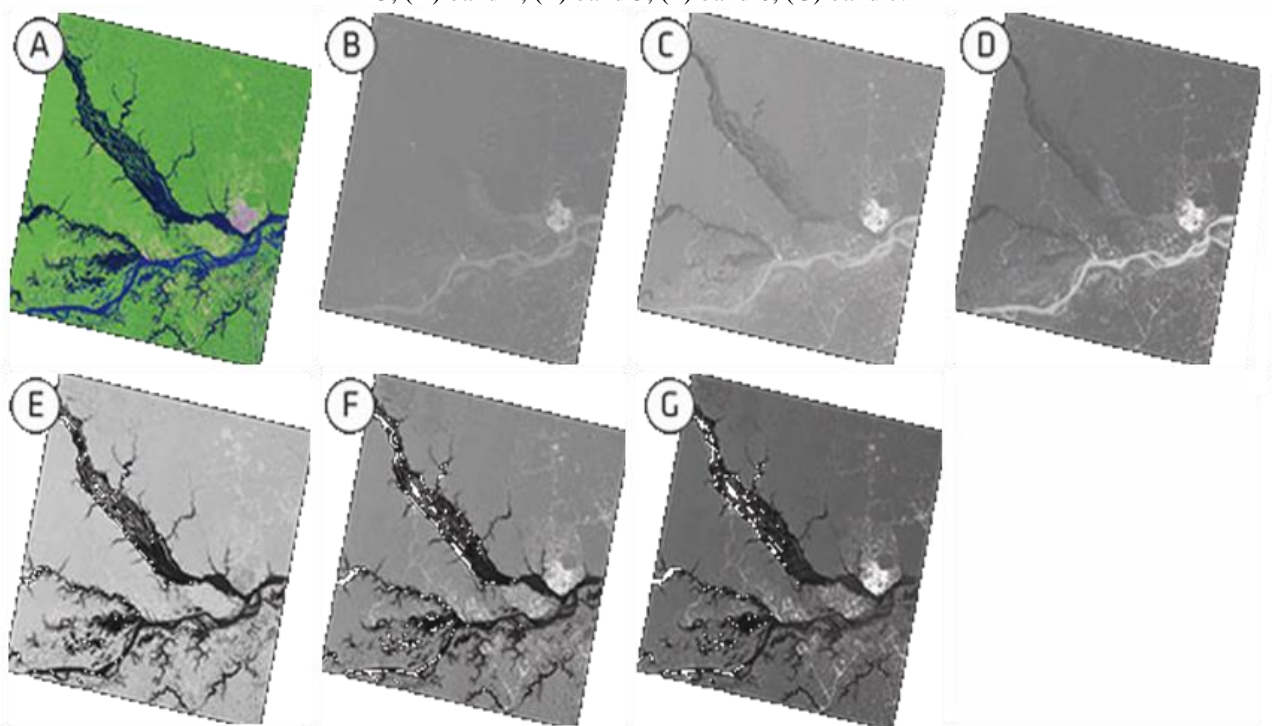
Obviously, the user should consider the type of data they are working with, especially when selecting endmembers. The user who is more familiar with the analysis of reflectance curves of different natural resources will probably feel more comfortable selecting endmembers when working with images converted to surface reflectance values because the shape of the curves will inform about the nature of the pixels selected as pure. This does not mean that they are not able to make a good selection by working with composite images of DNs. In this case, the shape of the curves would not be very useful but would not interfere with the performance of the mixing model.

Figure 3 - Example of spectral responses of vegetation, soil, and shade/water components.



Source: Shimabukuro and Ponzoni (2017).

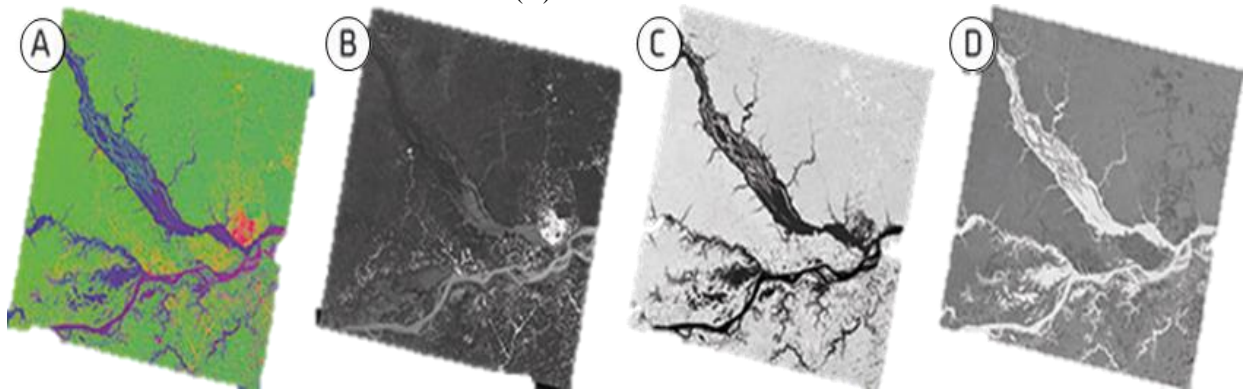
Figure 4 - (A) color composite (R6 G5 B4) of OLI/Landsat-8 for the image path 231 and row 062; (B) band 2; (C) band 3; (D) band 4; (E) band 5; (F) band 6; (G) band 7.



Source: Shimabukuro and Ponzoni (2017).

As a result, using the above images from the OLI/Landsat-8 sensor, it is observed that in the soil fraction image (Figure 5B), the brightest pixels are those that have the lowest levels of vegetation cover or less shade. While the vegetation fraction image presented in Figure 5C shows that the brightest pixels are the ones that have the highest amount of vegetation, while water bodies appear dark because they have no percentage of vegetation cover. A similar analysis can be done with images of other components.

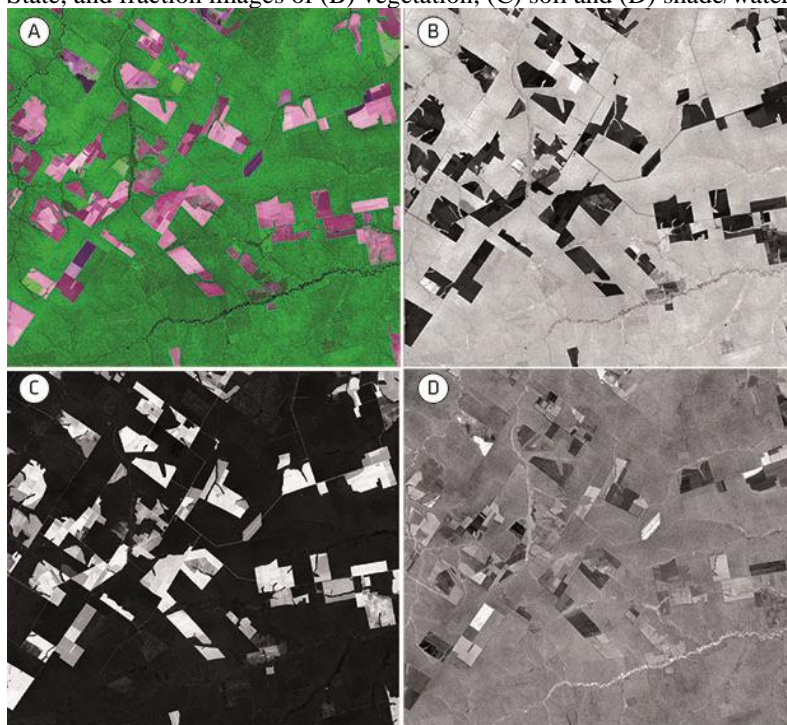
Figure 5 - (A) color composite of the fraction images (Rsoil Gvegetation Bshade/water) derived from OLI/ Landsat-8 sensor image for the Manaus region (Amazon State). The corresponding fraction images are: (B) soil, (C) vegetation and (D) shade/water fraction.



Source: Shimabukuro and Ponzoni (2017).

It is observed that the fraction images are monochromatic (grayscale), and the pixel-by-pixel values in each image are directly associated with the proportions (abundance) of each respective component of the scene selected for the spectral mixing model. Thus, the higher the value of a pixel in a vegetation fraction image (Figure 6B), for example, the greater the proportion of vegetation in the corresponding pixel (bright green in Figure 6A). The same interpretation applies to images of other components: the higher the value in a soil fraction image (Figure 6C), the greater proportion of soil in the corresponding pixel (magenta in Figure 6A), and the higher the value in a shade/water fraction image (Figure 6D), the greater the proportion of water or burned in the corresponding pixel (black or dark magenta in Figure 6A).

Figure 6 - (A) color composite (R6 G5 B4) of OLI/Landsat-8 part of the image path 226 and row 068 in Mato Grosso State, and fraction images of (B) vegetation, (C) soil and (D) shade/water.



Source: Shimabukuro and Ponzoni (2017).

The grayscale of fraction images is lighter with the highest proportion of endmembers in the pixel. The same convention is adopted for the error image associated with the model. The choice of convention is arbitrary, so that sometimes the tones of the image can be reversed to help in the visualization of patterns. For example, in case of shade/water fraction image, it is usually more intuitive when tones are inverted, so dark tones indicate less illumination (ADAMS; GILLESPIE, 2006). Fraction images can also be presented in

color composite (RGB) by selecting three images corresponding to the endmembers. In this case, the elongation of the image contrast can be applied to the visualization of the patterns but distorts the values of the proportion for quantitative use. To analyze a fraction image individually, it is more effective to present the higher proportions of brighter grayscale endmembers, to highlight the target of interest.

The literature presents a large number of studies on the use of linear spectral mixing model in diverse regions of the world, showing that this technique is consistent. In addition, the fraction images generated by this model are being used in different application areas, such as forests (SHIMABUKURO, 1987), agriculture (WHITE ET AL., 2002; YANG ET AL., 2007), land use and land cover (SHIMABUKURO et al., 2020), water (NOVO; SHIMABUKURO, 1994; ALCÂNTARA et al., 2009) and urban areas (WU; MURRAY, 2003).

As can be seen, the proportion of each endmember can be shown for each pixel, creating a useful image for photointerpretation. Fraction images are derived based on information from all multispectral bands used. Thus, for each type of application, the number of bands to be used can be limited, for example, in the analysis of deforested areas in the Amazon only three bands are sufficient: red, near-infrared and mid-infrared because they are spectral bands with low correlation and correspond to the bands conventionally used by several authors (SKOLE; TUCKER, 1993; SHIMABUKURO et al., 1998; INPE, 2008).

Therefore, the conversion of spectral data into fraction images through the linear spectral mixing model can result in a significant reduction in dimensionality of the data to be analyzed. For example, it is possible to use multiple sensor bands - six TM bands, seven MODIS bands, 242 Hyperion bands to generate a small number of fraction images (usually three or four endmembers).

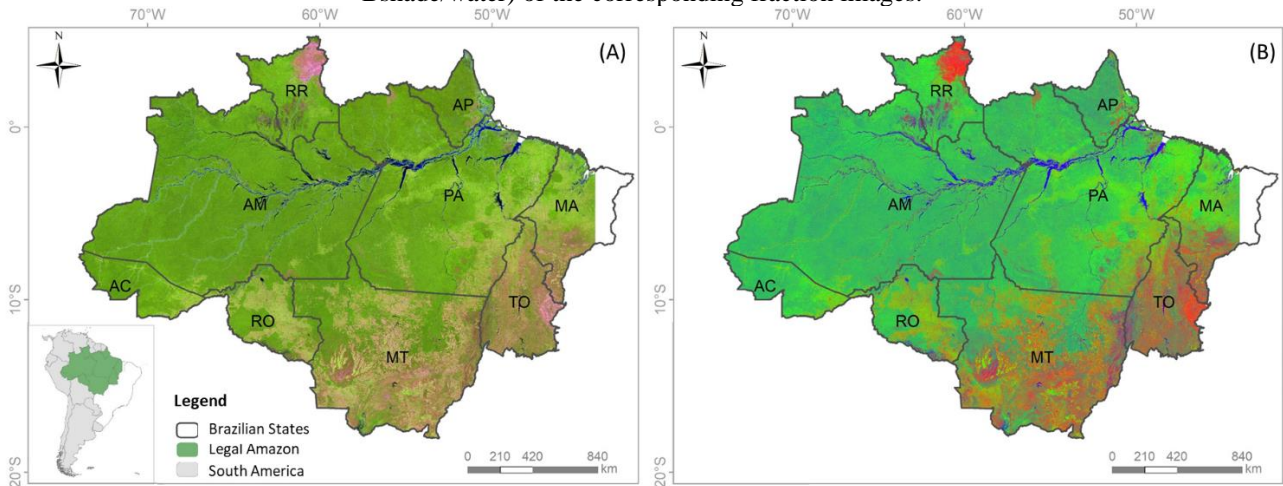
Now, once the proportions of the fraction images and the spectral responses of the endmembers are known, it is possible to recover the spectral responses of the pixels in each of the spectral bands used (SHIMABUKURO; SMITH, 1995; DUTRA et al., 2019). This procedure allows evaluating the performance of models to generate fraction images by calculating the error images.

Thus, based on the spectral mixing model, it is possible to calculate the error for each spectral band and generate the corresponding error images, since the response of the components and their proportions are known. This is one way to evaluate model performance, i.e., when the model is appropriate, error images show an aspect without any pattern. If there is a component that has not been considered in the mixture, it will be highlighted in the error images. Error images generally have low values according to the accuracy of the models used. Thus, these images are used to evaluate the quality of the defined models, i.e., whether the number of components was suitable for the analyzed scene.

6 APPLICATIONS IN THE AMAZON REGION

In this section, some examples of the use of fraction images derived from the linear spectral mixing model in environmental monitoring projects in the Brazilian Legal Amazon (BLA) (Figure 7) will be presented. Fraction images contributed to the development of small-scale researches, as well as in large-scale projects that use a large number of images.

Figure 7 - Location of the Brazilian Legal Amazon in South America and its respective states. (A) Color composite (Rmir Gmir Bred) from VIIRS-NPP images for the Legal Amazon, and (B) color composite (Rsoil Gvegetation Bshade/water) of the corresponding fraction images.



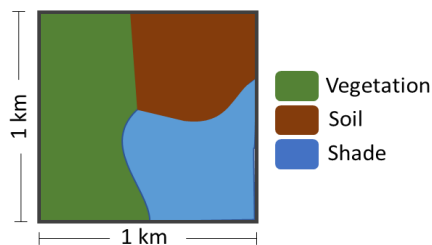
Source: The authors (2020).

6.1 Land Use and Land Cover Mapping

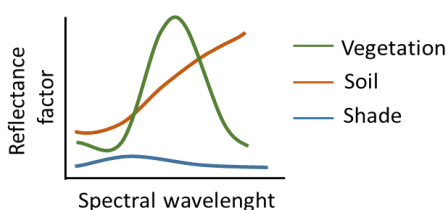
Fraction images of vegetation, soil, and shade/water were used to map land use and land cover on a national scale (SHIMABUKURO et al., 2020; ARAI et al., 2020) and on a regional scale (CASSOL et al., 2020). Figure 8 represents the conceptual idea used for agriculture mapping in the Mato Grosso State using multitemporal data from PROBA-V satellite using the maximum proportion of fraction images obtained in one-year time series (ARAI et al., 2020). In this example, considering the time series of approximately 288 images (72 scenes x four spectral bands) from the PROBA-V sensor, the application of LSMM allowed to identify areas destined for agriculture due to their characterization by homogeneous areas and a cyclic pattern between exposed soil (harvest and soil preparation) and vegetation cover. In this type of land use, unlike other land use and land cover types, the pixel presents a high proportion of soil fraction in a given period of the year and a high proportion of the vegetation fraction when the crop reaches the vegetative peak, supporting the use of maximum proportion of fractions approach. In addition, it was possible to reduce the volume of data to only three images containing the information of fraction images time series and then performing the steps of image classification.

Figure 8 - (A) Conceptual composition of a pixel with different elements within a pixel; (B) the subsequent theoretical spectral response of its elements to obtain the endmembers; and (C) theoretical representation of the temporal behavior of vegetation fraction images and the variation of the proportions over the study period.

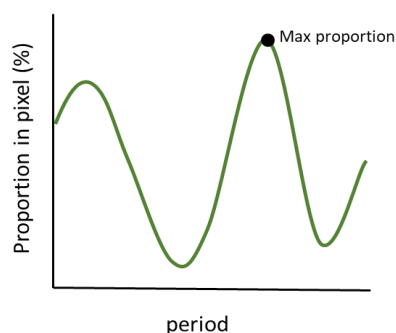
(A) Proba-V pixel



(B) Theoretical spectral response



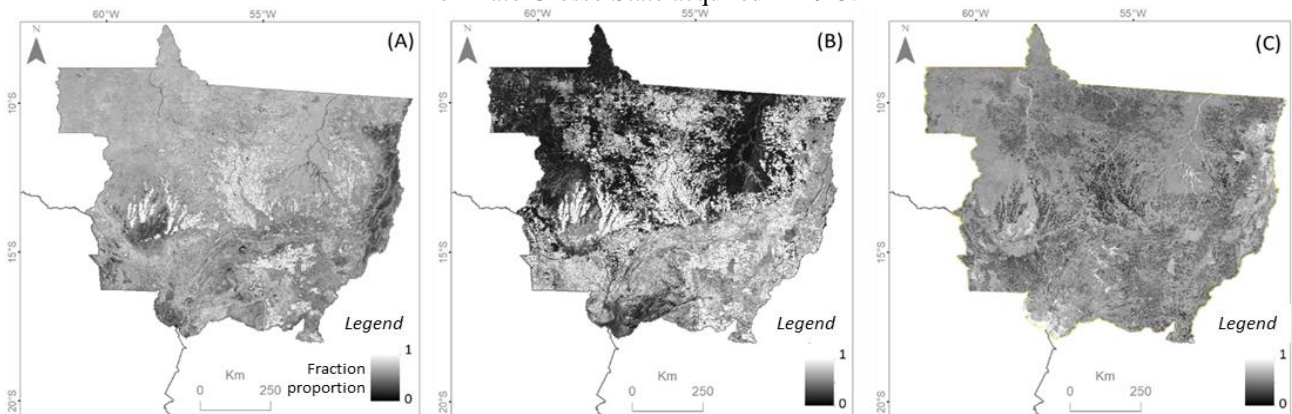
(C) Theoretical time-series of vegetation fraction images



Source: Arai et al. (2020).

Figure 9 presents an example of the maximum fraction of vegetation, soil, and shade/water images in Mato Grosso State derived from PROBA-V images acquired in 2015. The maximum vegetation fraction image (Figure 9A) shows agricultural areas highlighted, mainly soybean. On the other hand, maximum soil fraction image (Figure 9B) highlights the contrast between areas without or less vegetation (e.g. agriculture, deforestation and savanna areas whose vegetation is more spatially heterogeneous, in bright) and with dense vegetation (forest cover, in dark). In the maximum shade/water fraction image, the areas of water bodies and burned areas are highlighted.

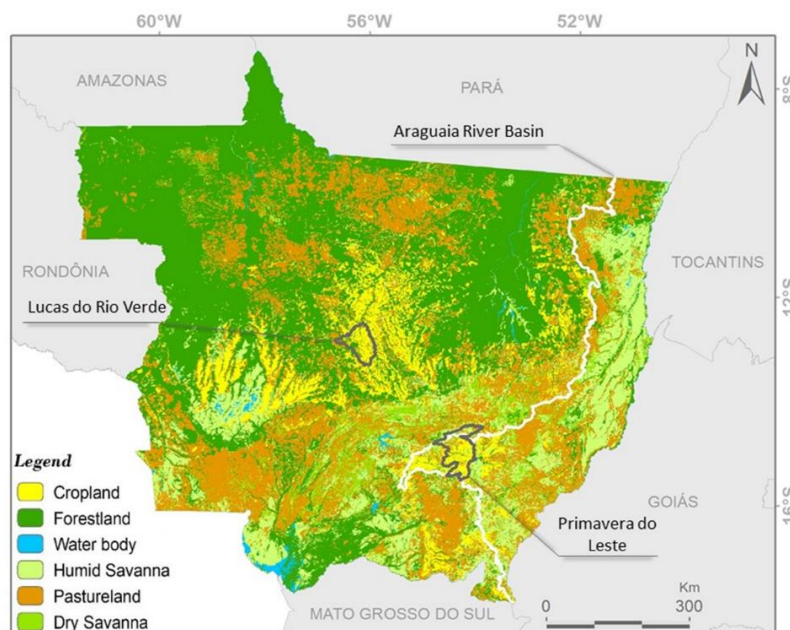
Figure 9 - (A) Maximum fraction images of vegetation, (B) soil, (C) and shade/water derived from PROBA-V images of Mato Grosso State acquired in 2015.



Source: Shimabukuro et al. (2020).

Figure 10 shows the mapping result of Mato Grosso State in 2015 using the maximum fraction images approach to separate the classes of land use and land cover, including pasture and savannah areas that present a high level of difficulty to distinguish them in automatic classifications. The authors performed the discrimination of classes based on variations of soil, vegetation, and shade fraction images, according to seasonality, instead of analyzing their spectral behaviors, which invariably change with a spatial resolution of the sensors. This means that each class has a typical annual behavior according to its increase or decrease of vegetation, soil, and shade proportions over a one-year time series (CASSOL et al., 2020).

Figure 10 - Map of land use and land cover of Mato Grosso State obtained based on the 2015 PROBA-V annual time series.

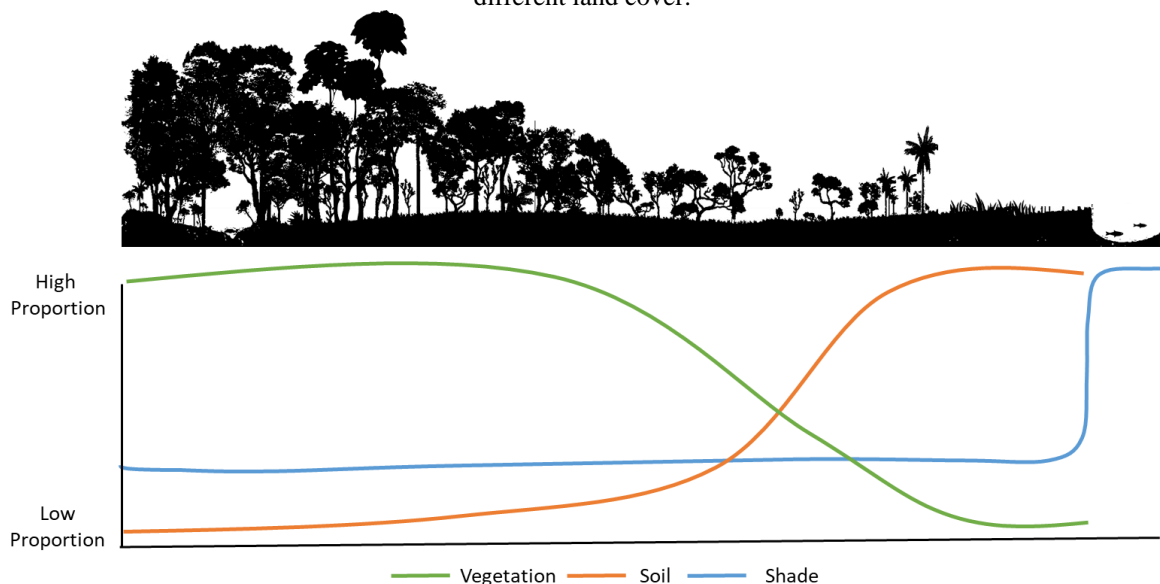


Source: Cassol et al. (2020).

As mentioned, vegetation, soil, and shade/water components are commonly used in applications with linear spectral mixing models as they are usually present in any land surface scene. These integrated components can provide important information for mapping and monitoring different land use and land cover types because they are related to the dynamics of targets on the surface and how they behave over time. Figure 11 represents, conceptually and illustratively, the dynamics of these three components in different land covers. In general, pixels that contain dense or spatially homogeneous vegetation, such as agriculture and forest, have a medium to high proportion of vegetation and low soil proportion. On the other hand, less dense or more sparse vegetation, such as degraded forests, herbaceous vegetation, or natural grasslands, presents an intermediate proportion of vegetation and soil due to the mixture of both components in the pixel. Water bodies, such as rivers and perennial lakes, present a high proportion of shade and almost zero proportions of vegetation and soil. Areas with exposed soil have a high proportion of soil and almost zero proportion of vegetation, which allows identifying, for example, deforested or degraded areas caused by selective logging (landing area and logging roads). Factors such as tree shadow and cloud shadow will also influence the proportion of shade fraction, as well as burned areas, due to their low reflectance in the spectrum region.

When analyzing the behavior of these three components over time, variations in the proportions of targets on the land surface resulting from seasonality dynamics and other factors such as clouds are observed. In agricultural areas, for example, variations in soil and vegetation proportions are observed during the growing season, harvesting, and pre-sowing phases. As well as variations are observed in seasonal vegetation, a characteristic observed in the savannas, for example. In addition, intermittent rivers and lakes present variation in shade and soil proportion. Then, fraction images can be applied for various purposes and knowledge of dynamics in space and time between components to support future research in this field of knowledge.

Figure 11 - Conceptual example of the proportion of main components of land surface (vegetation, soil, and shade) in different land cover.



Source: The authors (2020).

6.2 Deforestation Mapping

Deforestation in the Brazilian Legal Amazon has been a concern of several governmental and non-governmental organizations, especially in the last three decades (MORAN, 1981; SKOLE; TUCKER, 1993). Although there is no long history of human occupation in the BLA, almost 90% of deforestation for pastures and agriculture occurred between 1970 and 1988, as indicated by estimates based on satellite images (SKOLE et al., 1994).

Historically, the Brazilian territory was occupied along the coast, with most of its population concentrated in this region. In an attempt to change this occupation pattern, increasing the occupation in the interior of country, the federal capital was transferred from the coast, in Rio de Janeiro State, to the central region, in Brasilia, in the mid-1950s (MAHAR, 1988). This occupation policy required investments in infrastructure to connect Brasilia to other regions of the country. The construction of Belém-Brasília highway (BR-010), in 1958, was the dominant factor that triggered the main deforestation activities in the AML (MORAN et al., 1994; NEPSTAD et al., 1997). Subsequent events, such as the construction of BR-364, crossing the states of Mato Grosso, Rondônia and Acre, and the PA-150, in the state of Pará, encouraged other deforestation activities, converting forests into pasture and agriculture areas (MORAN, 1993).

To introduce the governance in the BLA, the "Superintendence of Development of the Amazon" (SUDAM) and the "Amazônia Bank" (BASA) were founded in 1966. Small producers were financed to encourage investment in agricultural projects (MORAN et al., 1994). Large producers were also financed through tax incentives in trade to convert forests into pasture areas (MORAN, 1993). The incentives granted to large producers were the main causes of deforestation; small producers had a smaller impact on deforestation due to the comparatively smaller practice of subsistence agriculture (FEARNSIDE, 1993).

Other activities of high economic value, such as mining and selective logging, have also contributed to the deforestation in the BLA (COCHRANE et al., 1999). Deforestation areas in the Brazilian Legal Amazon are concentrated in the so-called "arc of deforestation", located in the southern and eastern parts of the BLA, from Acre to Maranhão States (COCHRANE et al., 1999; ACHARD et al., 2002).

Since 1973, Brazil has access to remote sensing images of Landsat satellites, which allow quantifying the extent of natural resources and the change of the Amazon region. Based on the availability of these images, the Brazilian government began monitoring the Amazon rainforest to quantify deforestation areas at intervals of several years.

The Brazilian government has been conducting annual systematic monitoring of the Amazon rainforest since 1988, through the PRODES (Monitoring of the Brazilian Amazon rainforest by satellite) project, carried out by INPE, using images provided by the Landsat program. As the largest remote sensing project in the world to monitor deforestation activity in tropical forests, PRODES aims to evaluate all deforested areas within the 5 million square kilometers of the Brazilian Legal Amazon.

This project estimated approximately 810,000 km² of deforestation in the Brazilian Amazon by the year 2019 (INPE, 2020; ASSIS et al., 2019), corresponding to approximately 18% of the original forest extension. These data show annual deforestation rates that vary significantly in response to the country's political, economic and financial conditions, as well as the demands of the foreign market.

PRODES information is mainly based on images of sensors with a medium spatial resolution (30 m), such as those generated by the Landsat program, and with relatively low temporal resolution (acquisition frequency of 16 days), allowing annual monitoring of deforestation. A faster update of the forest change is not possible with these images due to the low frequency of cloudless image acquisition, which is a serious problem for the Amazon region, limiting the number of viable observations of the land surface. This prevents the government and environmental control agencies from making rapid and appropriate interventions to stop illegal deforestation activities.

In this manner, to monitor deforestation in a near-real-time, almost daily images of MODIS sensor onboard Terra and Aqua platforms were used. Thus, through the DETER project (Detection of deforestation in near-real-time), a new methodology based on MODIS images was developed for the rapid detection of deforestation in the Amazon (ANDERSON et al., 2005; SHIMABUKURO et al., 2006). Although MODIS is a moderate spatial resolution sensor and does not generate viable images to estimate the extent of deforestation, its data is valuable as indicators of change or as a warning product for the land surface policy management and control service. Currently, the project uses sensors data of higher spatial resolution, onboard the Sentinel, Landsat, and CBERS satellites.

6.2.1 DIGITAL PRODES PROJECT

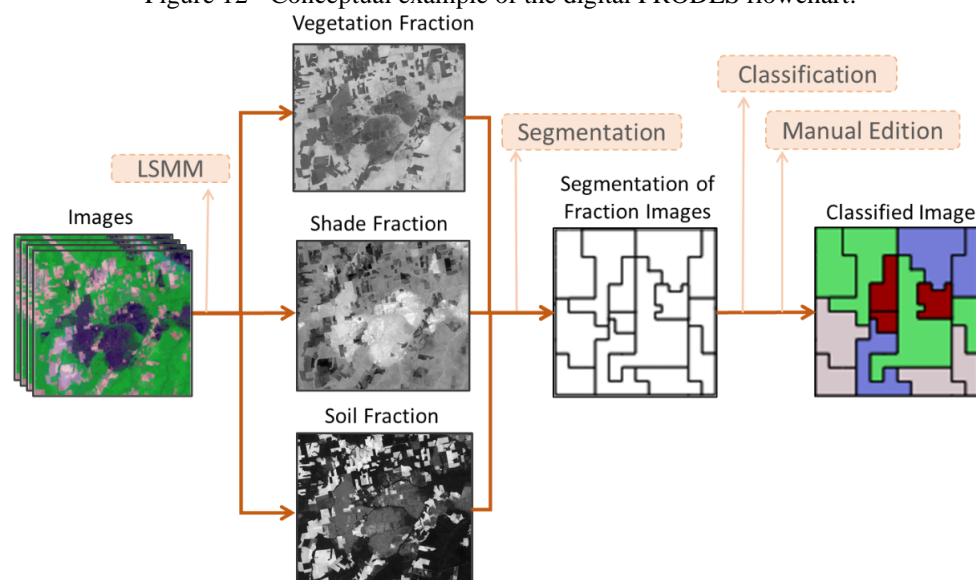
Since the end of 1970s, INPE has been conducting deforestation assessments at BLA using remote sensing images. These evaluations were made in conjunction with the former Brazilian Institute of Forest Development (IBDF), which was later incorporated into the Brazilian Institute of Environment and Renewable Natural Resources (IBAMA). The first evaluation was performed using images acquired by the MSS sensor, with four spectral bands and spatial resolution of 80 m, onboard Landsat satellites 1, 2 and 3, during the periods from 1973 to 1975 and from 1975 to 1978, using visual image interpretation (TARDIN et al., 1980)

From 1988, annual deforestation assessments were provided to the entire BLA using the TM sensor, six spectral bands with a spatial resolution of 30 m, onboard the Landsat 5 satellite, with better mapping quality due to its better spectral and spatial resolutions when compared to MSS data. The methodology applied to mapping deforested areas was based on the visual interpretation of color composites (R5 G4 B3) of TM images in printed format, on a scale of 1: 250,000. The visually interpreted polygons of the deforested areas were summed up to calculate the total deforested areas for each BLA state and presented in the tables form. This method, known as analogical PRODES, was carried out until 2003.

At the end of 1990s, a semi-automated methodology began to be developed using fraction images, called PRODES Digital (SHIMABUKURO et al., 1998). The PRODES Digital project is an automation of the activities developed in the PRODES project. In order that PRODES be able to detect deforestation in the BLA, an intact forest mask is updated annually by identifying a new deforestation event to exclude areas of non-forest vegetation and identifying other dynamic changes, such as secondary regeneration areas. The satellite images are selected for the period of July, August, and September, which is in the dry season period in the arc of deforestation and represents an atmospheric window when cloudless images are usually available. The red, near-infrared and mid-infrared spectral bands are used to generate fraction images (SHIMABUKURO et al., 1998).

Digital PRODES consists of the following methodological steps (Figure 12): (1) generation of vegetation, soil, and shade/water fraction images; (2) image segmentation based on the growing region algorithm; (3) classification of images based on unsupervised classifier; (4) mapping classes based on the following legend: forest, non-forest (vegetation that is not characterized by a forest structure), deforestation (accumulated deforestation until the previous year), hydrography, annual deforestation, and clouds; and (5) editing the classified map based on visual interpretation to minimize errors of omission and commission of automatic classification, in order to produce the final map of deforestation in digital format.

Figure 12 - Conceptual example of the digital PRODES flowchart.

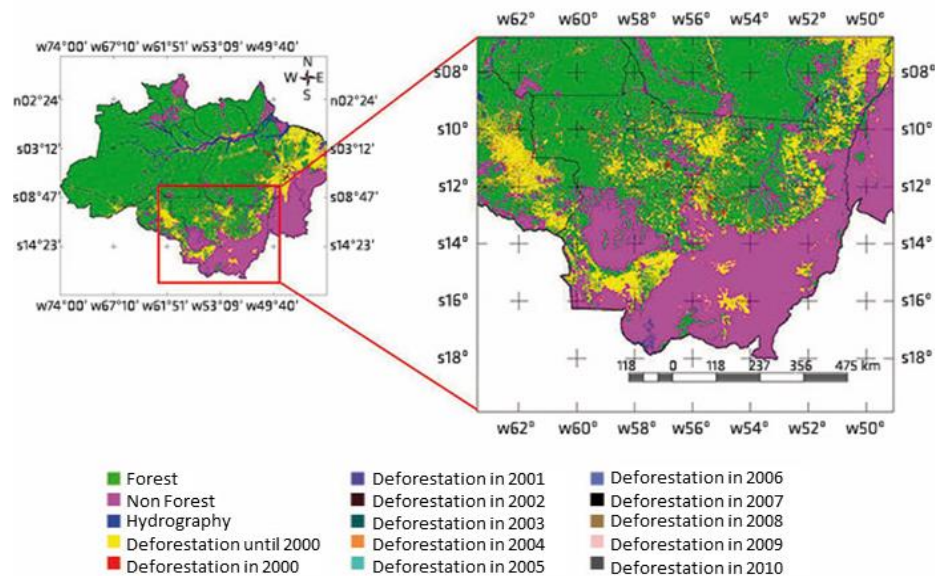


Source: The authors (2020).

The shade/water fraction image was used to characterize the total area deforested before 1997 in the BLA, according to the methodology proposed by Shimabukuro et al. (1998). In this case, the shade/water

fraction image was used for homogenizing forested areas (medium amount of shade) distinguishing from the other classes of land use (low amount of shade) such as exposed soil, pasture, and regeneration areas. Subsequently, the deforested areas were accumulated until the year 2000. For mapping the annual deforestation, soil fraction image is used because it highlights the areas without vegetation cover, which correspond to the annual increase in deforestation based on the high contrast between forested and deforested areas. The shade fraction images and vegetation can also be used for mapping annual deforestation since the forest and non-forest areas (newly cut forest) are very distinct in these images. But the soil fraction image better highlights the newly deforested areas. PRODES Digital allowed INPE to make available to the general community the information of deforested areas in the BLA (Figure 13), being recognized nationally and internationally (KINTISCH, 2007).

Figure 13 - Map of deforestation in the Brazilian Legal Amazon.



Source: Shimabukuro and Ponzoni (2017).

6.2.2 DETER PROJECT

Since 2004, the DETER project has been implemented with the objective of providing near-real-time detection of deforestation activities to support the Federal Government's action plan for the prevention and control the deforestation in the Brazilian Amazon. The procedure uses the methodology adopted by the PRODES Digital project but aims to detect deforestation activities in near-real-time, exploring high temporal resolution of MODIS sensors (ANDERSON et al., 2005; SHIMABUKURO et al., 2006).

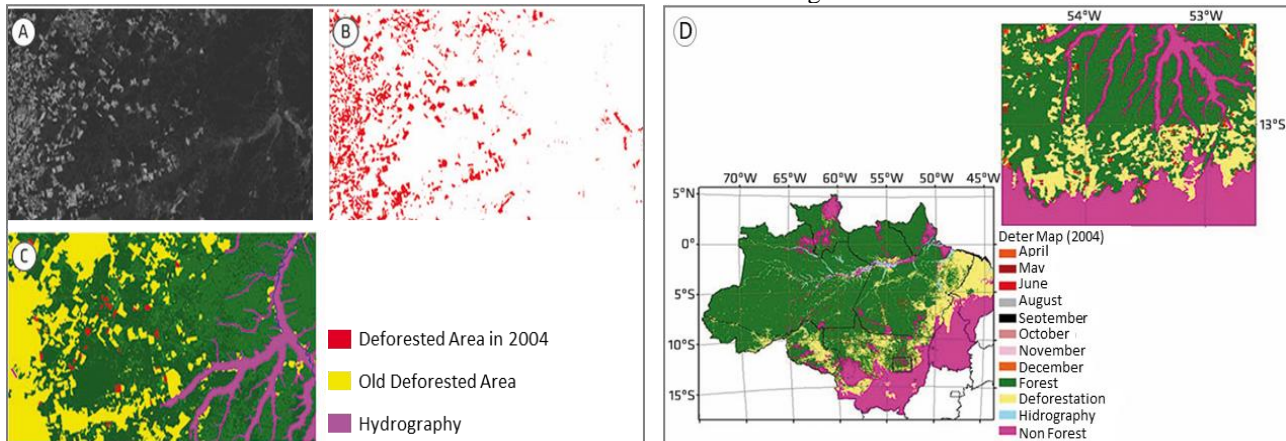
The first step in the DETER project method is to mask intact forests based on PRODES results in the previous year. The intact forest map is used as a reference to identify new real-time deforestation events throughout the year being analyzed. Monitoring activity with the images begins in January but becomes more effective after March when a larger number of images are available due to less cloud coverage in the Amazon region.

For the DETER project, MODIS daily images (MOD09 surface reflectance) were selected based on two criteria: (a) amount of cloud cover and (b) range within the zenith angle of the sensor, less than 35° (~1,400 km). The amount of clouds is initially evaluated according to the quick look images, followed by a more detailed analysis with the actual spatial resolution of MODIS images to be used. The BLA is covered by 12 MODIS tiles (V09 to V11 and H10 to H13).

From the set of seven bands of MOD09 product, bands 1 (red), 2 (NIR), and 6 (MIR) are used to generate fraction images of vegetation, soil, and shade/water, applying the linear spectral mixing model. Soil fraction images are then segmented, classified, mapped, and eventually edited by the interpreter, following the same procedures used in the PRODES Digital project. Deforested areas classified in the soil fraction images (Figure 14A and 14B) are overlaid to the forest mask, highlighting the areas of new deforestation

(red color in Figure 14C). This procedure is performed for each daily image acquired for the Brazilian Legal Amazon. The results of deforestation activities detected by DETER can be accumulated at different intervals, such as weekly, biweekly, and monthly (Figure 14D).

Figure 14 - (A) Soil fraction image (mosaic from April 22 to May 7, 2004); (B) result of the classification of soil fraction image; (C) MODIS image classification (mosaic from April 22 to May 7, 2004) over the total extension: August 2003 + deforestation until May 7, 2004; and (D) result of monitoring by DETER project, showing the monthly deforestation activities detected during 2004.



Source: Adapted from Shimabukuro and Ponzoni (2017).

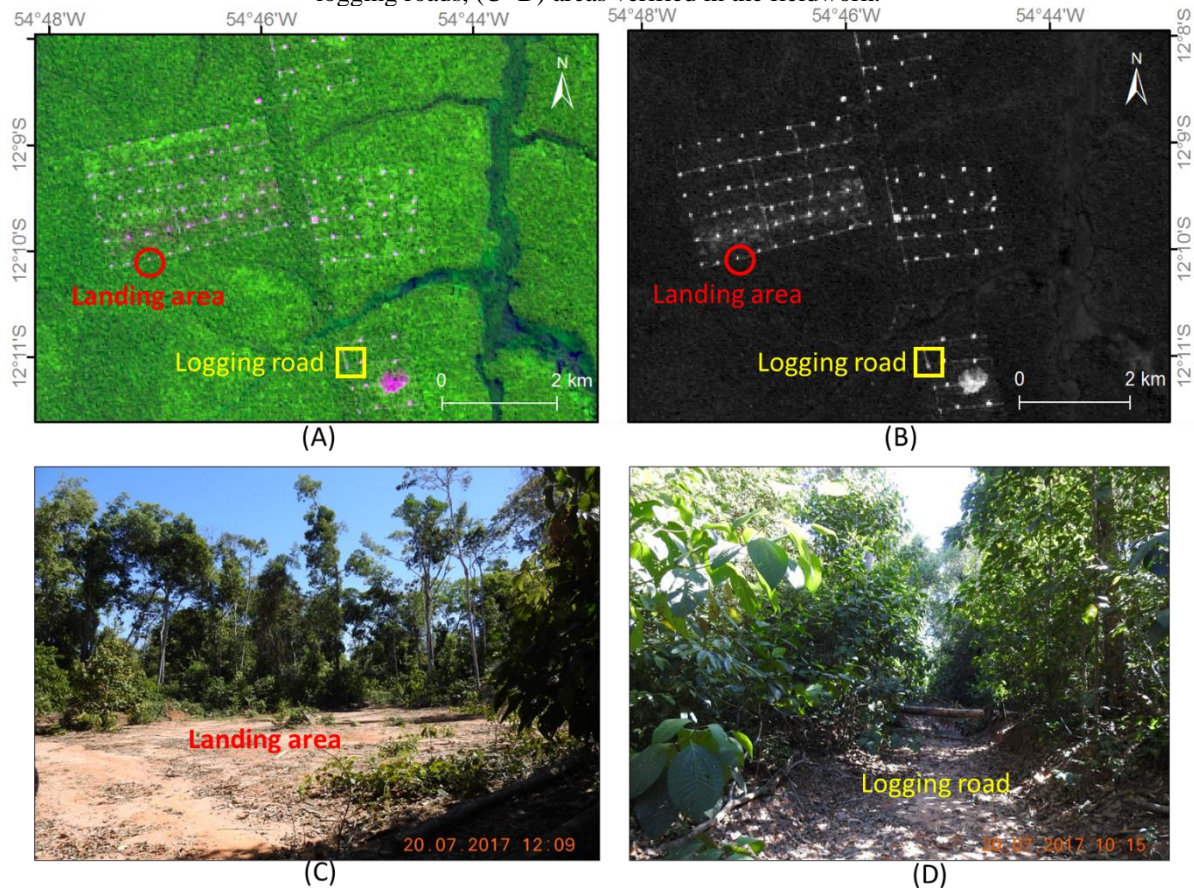
6.3 Detection of selective logging areas

The selective extraction of tree species with high commercial value is a practice used in areas of Amazon forest, requiring several studies for its detection and measurement, in addition to the evaluation of impacts on intact forests (ASNER et al., 2005; GROGAN et al., 2008; MATRICARDI et al., 2010; SHIMABUKURO et al., 2019).

Selective extraction is characterized by the opening of landing areas and trails or logging roads. Thus, with the use of medium spatial resolution images (coming from Landsat and Sentinel-2 satellites, for example), it is possible to detect these areas using soil fraction images generated by the linear spectral mixing model (SHIMABUKURO et al., 2019). The generation of fraction images for this purpose allows highlighting these areas of interest that are not always easily visualized in a color composite (Figure 15A) by visual inspection. As the forest becomes degraded with the removal of trees, the proportions of soil fractions increase due to the decrease in canopy cover and vegetation proportions decrease when comparing the proportions of these fractions in intact forests. Thus, the use of fraction images facilitates and increases the detection of landing and logging road areas due to the spectral behavior of these areas. This allows better discrimination of these areas and facilitates the subsequent classification process. Figure 15B shows the soil fraction image highlighting the areas characterized by selective logging, presenting landing area and logging roads, identified in the field as shown in Figure 15C-D.

Establishing an operational and efficient method to detect and monitor forest degradation by selective logging has been studied in the literature and many efforts have been reported using fraction images to map selective extraction (ASNER et al., 2005; ANWAR; STEIN, 2012). The development of indices such as NDFI (Normalized Difference Fraction Image) using vegetation fraction (GV – Green Vegetation), non-photosynthetic vegetation (NPV) and soil (SOUZA JR et al., 2005) images is useful for analyzing forest degradation.

Figure 15 - (A) Color composite RGB and (B) corresponding soil fraction image derived from a OLI/Landsat-8 image in an area in Mato Grosso State, highlighting selective logging areas, characterized by the presence of landing areas and logging roads, (C -D) areas verified in the fieldwork.



Source: Shimabukuro et al. (2019).

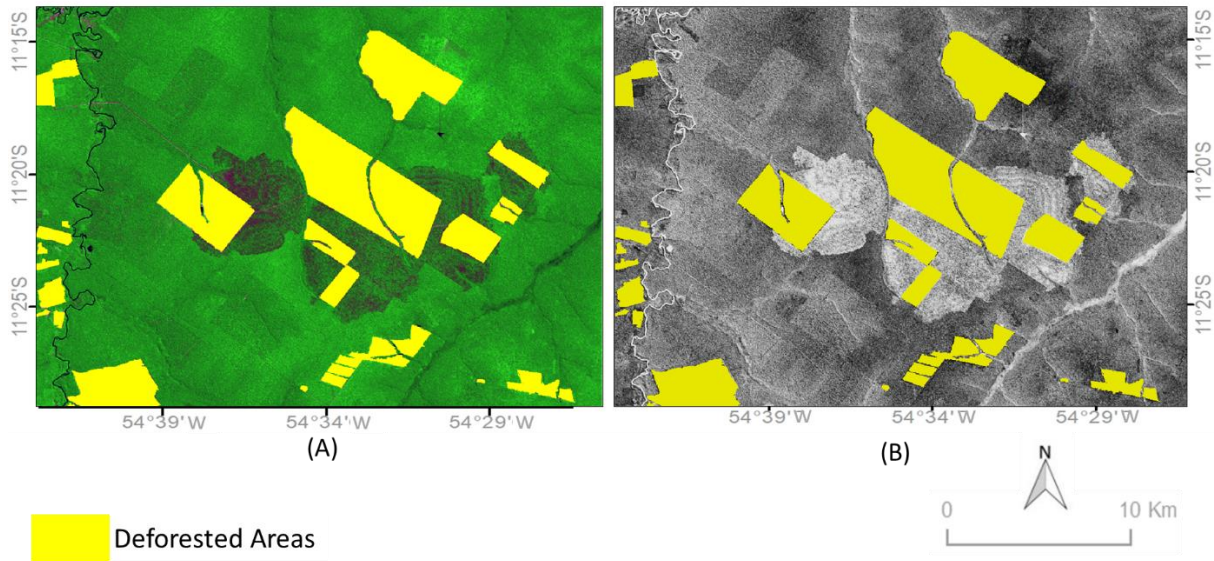
6.4 Burned areas mapping

Forest disturbances, such as selective logging and fire, are two of the main causes of forest degradation and carbon emissions in the Amazon region. Such disturbances induce changes in forest structure, species composition, biomass stocks and favor conversion to deforestation. With this, in addition to the ability of fraction images for the detection of deforested areas and selective logging, the fraction images are also able to identify another important anthropogenic action in the forest cover, such as fires.

For the initial interpretative phase of burned areas, using MODIS images, for example, information from the INPE Fire Monitoring Program (INPE, 2020b), which presents daily monitoring of critical points, can be used to provide a georeferenced database with the location of several hot-spots.

Figure 16A shows the location of burned areas in Mato Grosso State using a Landsat image, highlighting the areas mapped as deforestation (in yellow) that are masked to detect burned areas only in forest areas. Figure 16B represents the respective individual image of the shade/water fraction (SHIMABUKURO et al., 2019). Burned areas are identified by higher gray levels when compared to other targets in the shade/water fraction image, facilitating their discrimination. However, it is important to note that these areas can be confused with water bodies, and it is necessary to use a water mask to reduce inclusion errors by an automatic or semi-automatic method.

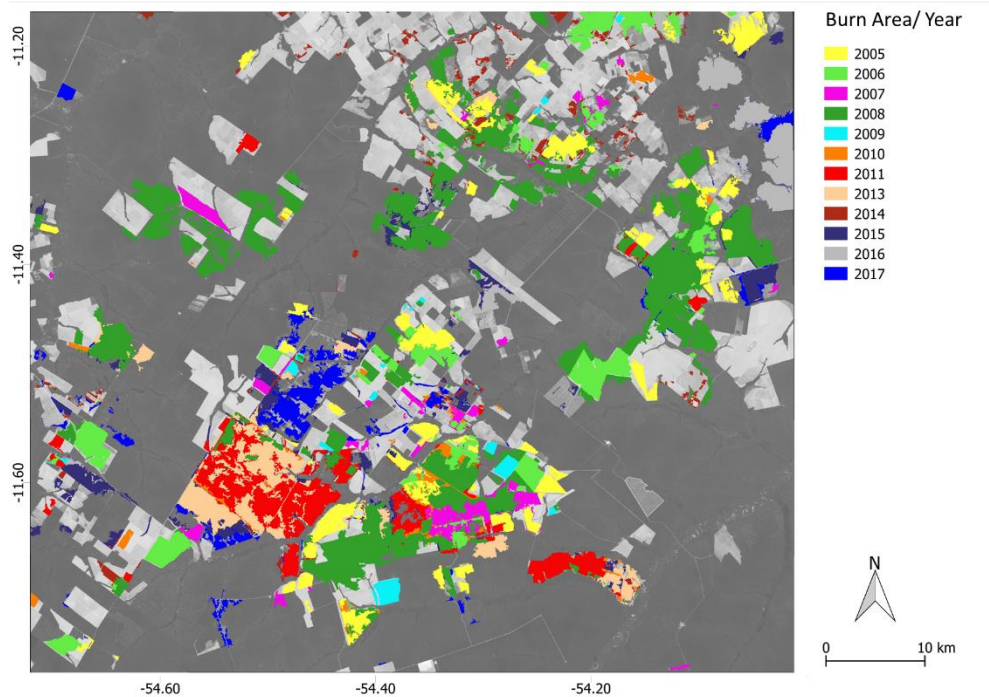
Figure 16 - Part of OLI/Landsat-8 image in Mato Grosso State: (A) displaying burned areas in forest, (B) and their shade/water fraction image highlighting areas of low reflectance.



Source: Shimabukuro et al. (2019).

Analyzing the annual results between 2005 and 2017 using Landsat satellites images, for example in Figure 17, the analysis of multitemporal fraction images of shade/water indicated the occurrence of approximately 957 km² of new forest burned areas in Mato Grosso State, i.e., areas of fire-degraded forest (SHIMABUKURO et al., 2019). In addition to these areas, it is also necessary to consider the occurrence of fire in previously deforested areas, where the burning activity serves as a traditional practice of land clearing for the implantation of agricultural crops or new pastures or even as a practice for improving pastures.

Figure 17 - Burned areas in Mato Grosso State identified in the images of Landsat TM and OLI sensors acquired between 2005 and 2017.



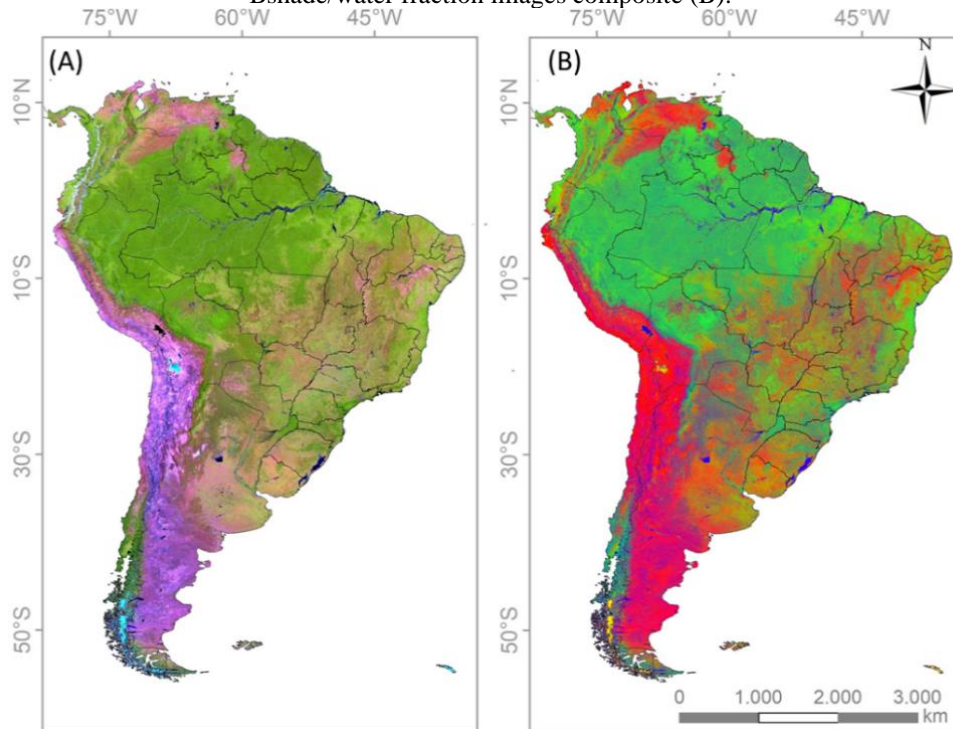
Source: Shimabukuro et al. (2019).

7 OPERATIONAL PERSPECTIVES

Some of the LSMM applications using fraction images derived punctually in time and at local and

regional scales were presented in this review work. Recently, some studies have demonstrated the applicability of LSMM in discriminating different targets of the land surface in a national (SHIMABUKURO et al., 2020) and global (ADAMI et al., 2018) scales (Figure 18); and, even more recently, there are studies that evidence the applicability of LSMM in analyses that use fraction images derived from intra-annual images (ARAI et al., 2020; CASSOL et al., 2020) or inter-annual (DUTRA, 2019).

Figure 18 - Rmir Gnrir Bred color composite from VIIRS-NPP images for South America (A) and its Rsoil Gvegetation Bshade/water fraction images composite (B).

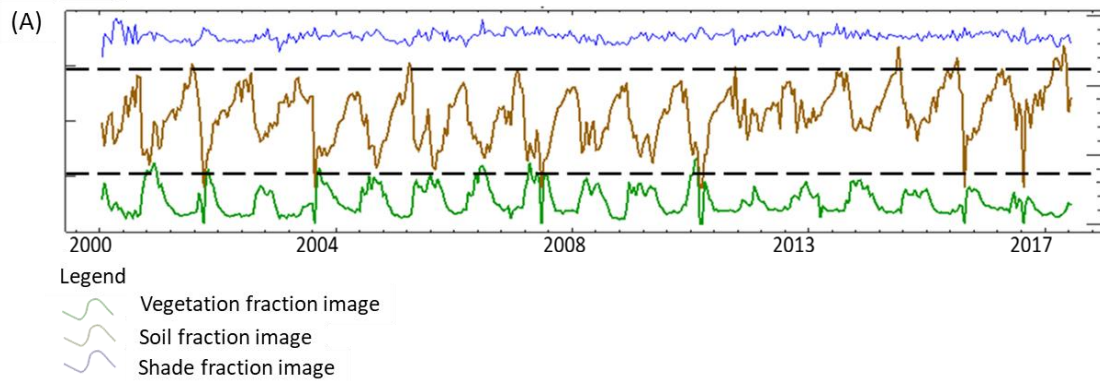


Source: The authors (2020).

In recent years there has been an exponential increase in the number of images available from remote sensors and, consequently, the increase in the number of studies based on time series analyses from selected samples over a given period of time (GALFORD et al., 2008; COUTO Jr. et al., 2012). Such analyses are usually associated with a large volume of data, and therefore it is necessary to use techniques that extract information efficiently or even reduce the dimensionality of the data without significant loss of information (BORGES; SANO, 2014). We also consider the use of techniques that do not present reduced sensitivity in regions of high biomass (e.g. tropical forests), and in addition to the contribution of soil effects, whose factors limit the application of certain vegetation indices (ADAMI et al., 2018).

Thus, fraction images resulting from the linear spectral mixing model applied in time series allow the quantification of proportions of each target in space and time and its variations. From a set of multitemporal images between 2000 and 2017, Dutra (2019) built profiles of space-time series of fraction images in order to observe the potentialities of these images for monitoring land use and land cover. As an example, it can be identified areas that presented evidence of degradation in native vegetation (Figure 19), as well as the silting of water bodies in periods characterized by extreme climatic events of drought from the increase of proportion of soil fraction.

Figure 19 - Example of time series profiles produced with fraction images of vegetation, soil, and shade between 2000 and 2017 period, without data filtering and in scale from 0 to 1 applied in a sample of degradation of native vegetation.



Source: Dutra (2019).

Thus, the use of temporal profiles of fraction images demonstrates the potentialities to analyze, for example, the relationship between the response of vegetation and the influence of climatic factors of precipitation and temperature in different phytophysionomies. This enables the use of statistical analyses, time-series algorithms for extraction of metrics and seasonality attributes, such as TIMESAT (EKLUNDH; JÖNSSON, 2012), in addition to methods capable of detecting pattern breaks in trend behavior, such as BFAST (Breaks For Additive Seasonal and Trend) (VERBESSELT et al., 2010).

In this context, the applications raised in this work corroborate the perspectives of establishing an operational methodology for mapping and monitoring land use and land cover at different geographical scales using the application of the linear spectral mixing model.

8 CONCLUSION

The spectral mixture can be linear and nonlinear. The linear model was discussed due to the ease of implementation with very satisfactory results. The linear spectral mixing model is a remote sensor data transformation technique, i.e., it converts spectral information into physical proportion of components within the pixel. This information about the proportion of components is represented in fraction images. Thus, the linear spectral mixing model is a data reduction technique and, in addition, highlights the information of these components in the pixel, facilitating later processes of classification and analysis. It is not a thematic classifier but provides useful information in the form of fraction images for a variety of applications in several areas of study.

In general, these components considered in the pixel are vegetation, soil, and shade/water, as the main elements present on the land surface. The vegetation fraction image presents information similar to vegetation indices such as NDVI and EVI, highlighting areas of vegetation cover; the soil fraction image highlights areas without vegetation cover; and the shade/water fraction image highlights water bodies and burned areas. Thus, the vegetation, soil, and shade/water fraction images were important to automate the PRODES project, carried out through the PRODES Digital project, providing both the estimation of deforested areas and the spatial distribution map of these areas, as well as the DETER project for the near real-time identification of forest disturbances. In addition to other applications related to land use and land cover mapping and forest disturbances such as selective logging and fire. The generation of time series of fraction images can contribute to the establishment of an operational methodology for mapping and monitoring land use and land cover at different geographical scales, and in different time analyses.

The review proposed in this work allowed to disseminate information and knowledge acquired from past applications, aiming to enable the filling of knowledge gaps and the improvement or development of reliable methodologies for several research themes in the field of remote sensing, during these 50 years of operation of the Brazilian Journal of Cartography (RBC).

In this context, the following questions arise for future research: What are the possibilities in the

development of comprehensive and reliable operational methods for mapping and monitoring the Brazilian Legal Amazon based on remote sensing data? How variations in the proportions of fraction images can be observed to elucidate the characterization of different targets on the land surface (e.g., forest regeneration, phytophysionomies, agriculture, water bodies, etc.)? What components can be analyzed as potential endmembers in future research in the Amazon region? Considering the sub-pixel-level analysis feature with fraction images, is it possible to obtain more accurate estimates in the calculation of areas? These are some of the suggestions in a range of possibilities and applications in scientific development for this field of knowledge.

Aknowledgements

This study was supported by the São Paulo Research Council (FAPESP-Grant 19806-3/2016). Y. E. S. thanks to the National Council for Scientific and Technological Development (CNPq – grant 303299/2018-5). A.C.D. thanks to the National Council for Scientific and Technological Development (CNPq – grant 380716/2019-4).

Authors contribution

Yosio Shimabukuro, Andeise Dutra and Egidio Arai participated in all stages of this review work, from its conception, bibliographic review, preparation of figures, tables, writing and revision of the manuscript.

Conflicts of interest

The authors declare that there are no conflicts of interest.

References

- ACHARD, F.; EVA, H. D.; STIBIG, H. J.; MAYAUX, P.; GALLEGO, J.; RICHARDS, T.; MALINGREAU, J. P. Determination of deforestation rates of the world's humid tropical forests. *Science*, 297(5583), pp. 999-1002, 2002. DOI: 10.1126/science.1070656.
- ADAMI, M.; BERNARDES, S.; ARAI, E.; FREITAS, R.M.; SHIMABUKURO, Y.E.; ESPÍRITO-SANTO, F.D.; RUDORFF, B.F.; ANDERSON, L.O. Seasonality of vegetation types of South America depicted by moderate resolution imaging spectroradiometer (MODIS) time series. *International Journal of Applied Earth Observation and Geoinformation*, v.69, p.148-163, 2018. DOI: 10.1016/j.jag.2018.02.010.
- ADAMS, J. B.; GILLESPIE, A. R. **Remote Sensing of Landscapes with Spectral Images: A Physical Modelling Approach**, 378 p., 2006. (Cambridge: Cambridge University Press).
- ADAMS, J. B.; SABOL, D.; KAPOV, V.; ALMEIDA, R.; ROBERTS, A.; SMITH, M. O.; GILLESPIE, A. R. Classification of multispectral images based on fractions of endmembers: application to land-cover change in the Brazilian Amazon. *Remote Sensing of Environment*, 52, pp. 137–154, 1995. DOI: 10.1016/0034-4257(94)00098-8.
- ADAMS, J. B.; SMITH, M. O.; JOHNSON, P. E. Spectral mixture modelling: a new analysis of rock and soil types at the Viking Lander I site. *Journal of Geophysical Research*, 91, pp. 8098–8112, 1986. DOI: 10.1029/JB091iB08p08098.
- ALCÂNTARA, E.; BARBOSA, C.; STECH, J.; NOVO, E. M.; SHIMABUKURO, Y. E. Improving the spectral unmixing algorithm to map water turbidity distributions. *Environmental Modelling and Software*, 24, pp. 1051–1061, 2009. DOI: 10.1016/j.envsoft.2009.02.013.
- ANDERSON, L. O.; SHIMABUKURO, Y. E.; DEFRIES, R. S.; MORTON, D. Assessment of deforestation

- in near real time over the Brazilian Amazon using multitemporal fraction images derived from Terra MODIS. **IEEE Geoscience and Remote Sensing Letters**, 2, pp. 315–318, 2005. DOI: 10.1109/LGRS.2005.850364.
- ANWAR, S.; STEIN, A. Detection and Spatial Analysis of Selective Logging with Geometrically Corrected Landsat Images. **International Journal of Remote Sensing**, 33 (24): 7820–7843, 2012. DOI: 10.1080/01431161.2012.701378.
- ASNER, G. P.; KNAPP, D. E.; BROADBENT, E. N.; OLIVEIRA, P. J.; KELLER, M.; SILVA, J. N. Selective logging in the Brazilian Amazon. **Science**, 310(5747), pp. 480–482, 2005. DOI: 10.1126/science.1118051.
- ATKINSON, P.; CUTLER, M.; LEWIS, H. Mapping subpixel proportional land cover with AVHRR imagery. **International Journal of Remote Sensing**, 18, pp. 917–935, 1997. DOI: 10.1080/014311697218836.
- ARAI, E.; SANO, E. E.; DUTRA, A. C.; CASSOL, H. L. G.; HOFFMANN, T. B.; SHIMABUKURO, Y. E. Vegetation Fraction Images Derived from PROBA-V Data for Rapid Assessment of Annual Croplands in Brazil. **Remote Sensing**, 12(7), p.1152, 2020. DOI: 10.3390/rs12071152.
- ASSIS, L. F. F. G.; FERREIRA, K. R.; VINHAS, L.; MAURANO, L.; ALMEIDA, C.; CARVALHO, A.; RODRIGUES, J.; MACIEL, A.; CAMARGO, C. TerraBrasilis: A Spatial Data Analytics Infrastructure for Large-Scale Thematic Mapping. **ISPRS International Journal of Geo-Information**, 8, 513, 2019. DOI: 10.3390/ijgi8110513.
- BASTIN, L. Comparison of fuzzy c-means classification, linear mixture modeling and MLC probabilities as tools for unmixing coarse pixels. **International Journal of Remote Sensing**, 18, pp. 3629–3648, 1997. DOI: 10.1080/014311697216847.
- BOARDMAN, J. W. **Automating spectral unmixing of AVIRIS data using convex geometry concepts...** (In Summaries 4th Annu. JPL Airborne Geoscience Workshop), JPL Publication 93–26, vol. 1, pp. 11–14, 1993.
- BORGES, E. F.; SANO, E. E.; MEDRADO, E. Radiometric quality and performance of TIMESAT for smoothing moderate resolution imaging spectroradiometer enhanced vegetation index time series from western Bahia State, Brazil. **Journal of Applied Remote Sensing**, 8(1), p.083580, 2014. DOI: 10.1117/1.JRS.8.083580.
- BURDEN, R. L.; FAIRES, J. D.; REYNOLDS, A. C. **Numerical analysis**. 2. ed. Boston, Massachusetts: Prindle, Weber and Schmidt, 1981.
- CASSOL, H. L. G.; ARAI, E.; SANO, E. E.; DUTRA, A. C.; HOFFMANN, T. B.; SHIMABUKURO, Y. E. Maximum Fraction Images Derived from Year-Based Project for On-Board Autonomy-Vegetation (PROBA-V) Data for the Rapid Assessment of Land Use and Land Cover Areas in Mato Grosso State, Brazil. **Land**, 9(5), p.139, 2020. DOI: 10.3390/land9050139.
- COCHRANE, M. A.; ALENCAR, A.; SCHULZE, M. D.; SOUZA JR., C. M.; NEPSTAD, D. C.; LEFEBVRE, P.; DAVIDSON, E. A. Positive Feedbacks on the fire dynamic of closed canopy tropical forests. **Science**, 284, 1832–1835, 1999. DOI: 10.1126/science.284.5421.1832.
- COUTO JUNIOR, A.F.; CARVALHO JUNIOR, O. A.; MARTINS, E. S. Séries temporais MODIS aplicadas em sucessão de culturas de soja (*Glycine max* (L.) Merrill) e milho (*Zea mays* L.) em sistema de plantio direto. **Revista Brasileira de Cartografia**, v. 64, p. 405–418, 2012.
- DE FREITAS, R. M.; HAERTEL, V.; SHIMABUKURO, Y. E. Modelo Linear de Mistura Espectral em Imagem de Moderada Resolução Espacial. **Boletim de Ciências Geodésicas**, v. 14, p. 55–71, 2008.
- DETMENDY, D.; PACE, W. A model for spectral signature variability for mixtures (Spectral signature variability model based on multispectral band scanner data and clustering experiments, discussing data processing algorithms). **Remote Sensing of Earth Resources**, p. 596–620, 1972.
- DUTRA, A. C. **Mapeamento e monitoramento da cobertura vegetal do estado da Bahia utilizando**

- dados multitemporais de sensores ópticos orbitais.** Dissertação (Mestrado em Sensoriamento Remoto) – Instituto Nacional de Pesquisas Espaciais, São José dos Campos, 2019.
- DUTRA, A. C.; SHIMABUKURO, Y. E.; ARAI, E. Linear spectral mixing model applied in images from PROBA-V sensor: A spatial multiresolution approach. **RAEGA—O Espaço Geográfico em Análise**, 46, 48–62, 2019. DOI: 10.5380/raega.v46i3.67098.
- EKLUNDH, L.; JÖNSSON, P. **TIMESAT 3.2 with parallel processing: software manual.** Lund: Lund University, 2012. 88p.
- FARRAND, W.; SINGER, R.; MERÉNYI, E. Retrieval of apparent surface reflectance from AVIRIS Data: a comparison of empirical line, radiative transfer, and spectral mixture methods. **Remote Sensing of Environment**, 47, pp. 311–321, 1994. DOI: 10.1016/0034-4257(94)90099-X.
- FEARNSIDE, P. M. Deforestation in Brazilian Amazonia: the effect of population and land tenure. **Ambio-Journal of Human Environment Research and Management**, 22(8), pp. 537-545, 1993.
- FOODY, G. M.; LUCAS, R. M.; CURRAN, P. J.; HONZAK, M. Non-linear mixture modelling without endmembers using an artificial neural network. **International Journal of Remote Sensing**, 18(4), p. 937-953, 1997. DOI: 10.1080/014311697218845.
- GALFORD, G. L.; MUSTARD, J. F.; MELILLO, J.; GENDRIN, A.; CERRI, C. C.; CERRI, C. E. P. Wavelet analysis of MODIS time series to detect expansion and intensification of row-crop agriculture in Brazil. **Remote Sensing of Environment**, v. 112, p. 576-587, 2008. DOI: 10.1016/j.rse.2007.05.017.
- GARCÍA-HARO, F.; SOMMNER, S.; KEMPER, T. A new tool for variable multiple endmember spectral mixture analysis (VMESMA). **International Journal of Remote Sensing**, 26, pp. 2135–2162, 2005. DOI: 10.1080/01431160512331337817.
- GROGAN, J.; JENNINGS, S. B.; LANDIS, R. M.; SCHULZE, M.; BAIMA, A. M.; LOPES, J. D. C. A.; SILVA, J. N. M. What loggers leave behind: Impacts on big-leaf mahogany (*Swietenia macrophylla*) commercial populations and potential for post-logging recovery in the Brazilian Amazon. **Forest Ecology and Management**, 255(2), pp. 269-281, 2008. DOI: 10.1016/j.foreco.2007.09.048.
- HALLUM, C. R. On a model for optimal proportions estimates for category mixtures. **Remote Sensing of Environment**, 951, 1972.
- HAPKE, B. **Theory of Reflectance and Emittance Spectroscopy.** (Cambridge, MA: Cambridge University Press), 1993.
- HEIMES, F. J. **Effects of scene proportions on spectral reflectance in lodgepole pine.** (In Doctoral dissertation, Colorado State University), 1977.
- HORWITZ, H. M.; NALEPKA, R. F.; HYDE, P. D.; MORGENSTERN, J. P. **Estimating the proportions of objects within a single resolution element of a multispectral scanner.** Ann Arbor: University of Michigan, Contract NAS-9-9784, 1971.
- ICHOKU, C.; KARNIELI, A. A review of mixture modeling techniques for sub-pixel land cover estimation. **Remote Sensing Reviews**, 13, pp. 161–186, 1996. DOI: 10.1080/02757259609532303.
- INPE, 2008. **Monitoramento da cobertura florestal da Amazônia por Satélites. Sistemas PRODES, DETER, DEGRAD e QUEIMADAS 2007-2008.** INPE, p. 47. Available in: http://www.obt.inpe.br/OBT/assuntos/programas/amazonia/deter/pdfs/metodologia_v2.pdf. Access in: aug. 2020.
- INPE - Instituto Nacional de Pesquisas Espaciais. Coordenação Geral de Observação da Terra. **Programa de Monitoramento da Amazônia e Demais Biomas. Desmatamento – Amazônia Legal.** Available in: <http://terrabrasilis.dpi.inpe.br/downloads/>. Access in: may 2020.
- INPE - Instituto Nacional de Pesquisas Espaciais. **Portal do Monitoramento de Queimadas e Incêndios, 2020b.** Available in: <http://queimadas.dgi.inpe.br/queimadas/aq1km/>. Access in: may 2020.
- KESHAVA, N. A survey of spectral unmixing algorithms. **Lincon Laboratory Journal**, 14, pp. 55–78, 2003. Available in: https://archive.ll.mit.edu/publications/journal/pdf/vol14_no1/14_1survey.pdf. Access

in: may 2020.

- KESHAVA, N.; MUSTARD, J. F. Spectral unmixing. **IEEE Processing Magazine**, 2, pp. 44–57, 2002. DOI: 10.1109/79.974727.
- KINTISCH, E. Carbon Emissions: Improved Monitoring of Rainforests Helps Pierce Haze of Deforestation. **Science**, 316, 5824, p. 536–537, 27 abr. 2007. DOI: 10.1126/science.316.5824.536.
- MAHAR, D. J. **Deforestation in Brazil's Amazon region: Magnitude, rate and causes**. The World Bank, New York, 1988. Available in: <http://documents1.worldbank.org/curated/en/304691468770373897/pdf/multi-page.pdf>. Access in: may 2020.
- MATRICARDI, E. A.; SKOLE, D. L.; PEDLOWSKI, M. A.; CHOMENTOWSKI, W.; FERNANDES, L. C. Assessment of tropical forest degradation by selective logging and fire using Landsat imagery. **Remote Sensing of Environment**, 114(5), pp. 1117-1129, 2010. DOI: 10.1016/j.rse.2010.01.001.
- MEYER, T.; OKIN, G. S. Evaluation of spectral unmixing techniques using MODIS in a structurally complex savanna environment for retrieval of green vegetation, nonphotosynthetic vegetation, and soil fractional cover. **Remote Sensing of Environment**, 161, p. 122-130, 2015. DOI: 10.1016/j.rse.2015.02.013.
- MORAN, E. F. Developing the Amazon. **Indiana Univ. Press**, 1981. DOI: 10.1086/ahr/87.5.1507.
- MORAN, E. F. Deforestation and land use in the Brazilian Amazon. **Human Ecology**, 21(1), pp. 1-21, 1993.
- MORAN, E. F.; BRONDIZIO, E.; MAUSEL, P.; WU, Y. Integrating Amazonian vegetation, land-use, and satellite data. **BioScience**, 44(5), pp. 329-338, 1994.
- NEPSTAD, D. C.; KLINK, C. A.; UHL, C.; VIEIRA, I. C.; LEFEBVRE, P.; PEDLOWSKI, M.; HOMMA, A. Land-use in Amazonia and the cerrado of Brazil. Embrapa Amazônia Oriental-Artigo em periódico indexado (ALICE), **Ciência e Cultura**, São Paulo, v. 49, n. 1/2, p. 73-86, 1997. Available in: <http://www.alice.cnptia.embrapa.br/alice/handle/doc/1030465>. Access in: may 2020.
- NOVO, E.; SHIMABUKURO, Y. E. Spectral mixture analysis of inland tropical waters. **International Journal of Remote Sensing**, 15, pp. 1351–1356, 1994. DOI: 10.1080/01431169408954169.
- PANIZZA, A. C.; FONSECA, F. P. Técnicas de interpretação visual de imagens. **GEOUSP - Espaço e Tempo**, São Paulo, 30, pp. 30-43, 2011. DOI: 10.11606/issn.2179-0892.geousp.2011.74230.
- PLAZA, A.; MARTÍNEZ, P.; PÉREZ, R.; PLAZA, J. Spatial/spectral *endmember* extraction by multidimensional morphological operations. **IEEE Transactions on Geoscience and Remote Sensing**, 40, pp. 2025–2041, 2002. DOI: 10.1109/TGRS.2002.802494
- PLAZA, A.; MARTÍNEZ, P.; PÉREZ, R.; PLAZA, J. A quantitative and comparative analysis of *endmember* extraction algorithms from hyperspectral data. **IEEE transactions on geoscience and remote sensing**, 42(3), pp. 650-663, 2004. DOI: 10.1109/TGRS.2003.820314.
- QUINTANO, C.; FERNÁNDEZ-MANSO, A.; SHIMABUKURO; Y. E.; PEREIRA, G. Spectral unmixing, **International Journal of Remote Sensing**, 33, 17, 5307-5340, 2012. DOI: 10.1080/01431161.2012.661095.
- RANSON, K. J. **Computer assisted classification of mixtures with simulated spectral signatures** (In Doctoral dissertation, Colorado State University), 1975.
- ROBERTS, D. A.; SMITH, M.; ADAMS, J. Green vegetation, nonphotosynthetic vegetation, and soils in AVIRIS data. **Remote Sensing of Environment**, 44, pp. 255–269, 1993. DOI: 10.1016/0034-4257(93)90020-X.
- ROSIN, P. Robust pixel unmixing. **IEEE Transactions on Geoscience and Remote Sensing**, 39, pp. 1978–1983, 2001. DOI: 10.1109/36.951088.
- SHIMABUKURO, Y. E. **Shade images derived from linear mixing models of multispectral measurements of forested areas**. Dissertation (Doctor of Philosophy) - Fort Collins, CO: Colorado State University, 1987.

- SHIMABUKURO, Y. E.; SMITH, J. A. The least squares mixing models to generate fraction images derived from remote sensing multispectral data. **IEEE Transactions on Geoscience and Remote Sensing**, v. 29, n. 1, pp. 16-20, Jan. 1991. DOI: 10.1109/36.103288.
- SHIMABUKURO, Y. E.; SMITH, J. A. Fraction images derived from Landsat TM and MSS data for monitoring reforested areas. **Canadian Journal of Remote Sensing**, v. 21, n. 1, p. 67-74, 1995. DOI: 10.1080/07038992.1995.10874599.
- SHIMABUKURO, Y. E.; BATISTA, G. T.; MELLO, E. M.; MOREIRA, J. C.; DUARTE, V. Using shade fraction image segmentation to evaluate deforestation in Landsat Thematic Mapper images of the Amazon Region. **International Journal of Remote Sensing**, 19, pp. 535-541, 1998. DOI: /10.1080/014311698216152.
- SHIMABUKURO, Y. E.; DUARTE, V.; ANDERSON, L. O.; VALERIANO, D. M.; ARAI, E.; FREITAS, R. M.; RUDORFF, B. F. T.; MOREIRA, M. A. Near real time detection of deforestation in the Brazilian Amazon using MODIS imagery. **Ambiente e Água**, 1, pp. 37-47, 2006. DOI:10.4136/1980-993X.
- SHIMABUKURO, Y.E.; ARAI, E.; DUARTE, V.; JORGE, A.; SANTOS, E. G. D.; GASPARINI, K. A. C.; DUTRA, A. C. Monitoring deforestation and forest degradation using multi-temporal fraction images derived from Landsat sensor data in the Brazilian Amazon. **International Journal of Remote Sensing**, 40(14), pp. 5475-5496, 2019. DOI: 10.1080/01431161.2019.1579943.
- SHIMABUKURO, Y.E.; ARAI, E.; DUARTE, V.; DUTRA, A. C.; CASSOL, H. L. G.; SANO, E. E.; HOFFMANN, T. B. Discriminating Land Use and Land Cover Classes in Brazil Based on the Annual PROBA-V 100 m Time Series. **IEEE Journal of Selected Topics in Applied Earth Observations and Remote Sensing**, vol. 13, pp. 3409-3420, 2020. DOI: 10.1109/JSTARS.2020.2994893.
- SHIMABUKURO, Y. E.; PONZONI, F. J. **Mistura Espectral: modelo linear e aplicações**. Oficina de Textos, 2017.
- SKOLE, D. L.; CHOMENTOWSKI, W. H.; SALAS, W. A.; NOBRE, A. D. Physical and human dimensions of deforestation in Amazonia. **BioScience**, 44(5), pp. 314-322, 1994. DOI: 10.2307/1312381.
- SKOLE, D.; TUCKER, C. Tropical deforestation and habitat fragmentation in the Amazon: satellite data from 1978 to 1988. **Science**, 260(5116), pp. 1905-1910, 1993. DOI: 10.1126/science.260.5116.1905.
- SMITH, M. O.; JOHNSON, P. E.; ADAMS, J. B. Quantitative determination of mineral types and abundances from reflectance spectra using principal components analysis. **Journal of Geophysical Research**, 90, pp. 797-804, 1985. DOI: 10.1029/JB090iS02p0C797.
- SOUZA JR, C. M.; ROBERTS, D. A.; COCHRANE, M.A. Combining spectral and spatial information to map canopy damage from selective logging and forest fires. **Remote Sensing of Environment**, 98, 329-343, 2005. DOI: g/10.1016/j.rse.2005.07.013.
- TARDIN, A. T.; LEE, D. C. L.; SANTOS, R. J. R.; OSSIS, O. R.; BARBOSA, M. D. S.; MOREIRA, M. D. L.; SANTOS FILHO, C. P. **Subprojeto desmatamento**. IBDF/CNPq-INPE, Instituto de Pesquisas Espaciais, São José dos Campos, Brazil, 1980.
- VERBESSELT, J.; HYNDMAN, R.; NEWNHAM, G.; CULVENOR, D. Detecting trend and seasonal changes in satellite image time series. **Remote Sensing of Environment**, n. 114, p. 106-115, 2010. DOI: 10.1016/j.rse.2009.08.014.
- WHITE, K.; LIVINGSTONE, I.; GURNEY, S.; DEARING, J.; BATEMAN, M. Postprocessing of mineral mixture maps for mapping surficial materials: the example of the Matmata loess, southern Tunisia. **International Journal of Remote Sensing**, 23, pp. 3091-3106, 2002. DOI: 10.1080/01431160110104674.
- WU, C.; MURRAY, A. T. Estimating impervious surface distribution by spectral mixture analysis. **Remote Sensing of Environment**, 84, pp. 493-505, 2003. DOI: 10.1016/S0034-4257(02)00136-0.
- YANG, C.; EVERITT, J. H.; BRADFORD, J. M. Airborne hyperspectral imagery and linear spectral unmixing for mapping variation in crop yield. **Precision Agriculture**, 8, pp. 279-296, 2007. DOI:

10.1007/s11119-007-9045-x.

Author's Biography



Yosio Edemir Shimabukuro received BSc in Forestry Engineering from the Federal Rural University of Rio de Janeiro (UFRRJ) in 1972; MSc in Remote Sensing from the National Institute for Space Research (INPE) in 1977; and PhD from Colorado State University, USA in 1987. From January 1992 to March 1994, he was a visiting researcher at NASA's Goddard Space Flight Center, USA. Since 1973, he has been at INPE, using satellite and terrestrial remote sensing data for land cover analysis. He has been applying techniques and models of geographic information system and remote sensing to study environmental changes in different biomes in Brazil. He is 1A Researcher of the National Council for Scientific and Technological Development (CNPq).



Andeise Cerqueira Dutra was born in Bahia State, Brazil. She received the BSc in Forestry Engineering from the Federal University of Recôncavo da Bahia (UFRB) in 2017 and the MSc in Remote Sensing from the National Institute for Space Research (INPE) in 2019. She is currently a fellowship from the National Council for Scientific and Technological Development (CNPq) on the project of the Cerrado biome fire risk system (SIRI). Her interests are species phenology, land-use and land-cover changes, and monitoring of vegetation over different biomes in Brazil using remote sensing and geographic information system techniques.



Egidio Arai received the Technologist degree in Data Processing from the University of Taubaté (UNITAU), Taubaté, in 1986, MSc degree in Applied Computing, in 2002, and Ph.D. degree in Remote Sensing, in 2011, from the National Institute for Space Research (INPE), São José dos Campos, Brazil. He is currently a Senior Technologist at INPE. His interests are computer science and remote sensing, acting on the following subjects: image processing, remote sensing, time series, tropical ecosystems and environmental sciences, forest resources, and computer systems.



Esta obra está licenciado com uma Licença [Creative Commons Atribuição 4.0 Internacional](https://creativecommons.org/licenses/by/4.0/) – CC BY. Esta licença permite que outros distribuam, remixem, adaptem e criem a partir do seu trabalho, mesmo para fins comerciais, desde que lhe atribuam o devido crédito pela criação original.